Lymphoid origin of intrinsically activated plasmacytoid dendritic cells in mice.

Alessandra M. Araujo[1*], Joseph D. Dekker[1*^], Kendra Garrison[1], Zhe Su[2], Catherine Rhee[3], Zicheng Hu[3], Bum-Kyu Lee[3], Daniel Osorio Hurtado[2], Jiwon Lee[1], Vishwanath R. Iyer[3], Lauren I. R. Ehrlich[3], George Georgiou[1,3], Gregory C. Ippolito[3], S. Stephen Yi[2^], and Haley O. Tucker[3^].

[1] Department of Chemical Engineering, The University of Texas at Austin, Austin TX, USA.

[2] Department of Biomedical Engineering, and Livestrong Cancer Institutes, The University of Texas at Austin, Austin TX, USA.

[3] Department of Molecular Biosciences, The University of Texas at Austin, Austin TX, USA.

Running Title: pDC lymphoid development

^Corresponding Authors:

Haley O. Tucker, Department of Molecular Biosciences. The University of Texas at Austin, 1 University Station A5000, Austin TX 78712, USA. Phone: (512) 475-7706;
Fax (512) 475-7707; E-mail: haleytucker@austin.utexas.edu

Joseph D. Dekker, Department of Molecular Biosciences. The University of Texas at Austin, 1 University Station A5000, Austin TX 78712, USA. Phone: (505)4637855; ORCID: orcid.org/0000-0002-2068-3529; E-mail: joedekker@gmail.com

S. Stephen Yi, Livestrong Cancer Institutes, and Department of Biomedical Engineering, The University of Texas at Austin, Austin TX 78712, USA. Phone: (512) 495-5245; E-mail: stephen.yi@austin.utexas.edu;

Abstract

We identified a novel mouse plasmacytoid dendritic cell (pDC) lineage derived from the common lymphoid progenitors (CLPs) that is dependent on expression of *Bcl11a*. These CLP-derived pDCs, which we refer to as "B-pDCs", have a unique gene expression profile that includes hallmark B cell genes, normally not expressed in conventional pDCs. Despite expressing most classical pDC markers such as SIGLEC-H and PDCA1, B-pDCs lack IFN-α secretion, exhibiting a distinct inflammatory profile. Functionally, B-pDCs induce T cell proliferation more robustly than canonical pDCs following Toll-like receptor 9 (TLR9) engagement. B-pDCs, along with another homogeneous subpopulation of myeloid derived pDCs, display elevated levels of the cell-surface receptor tyrosine kinase AXL, mirroring human AXL^+ transitional DCs in function and transcriptional profile. Murine B-pDCs therefore represent a phenotypically and functionally distinct CLP-derived DC lineage specialized in T cell activation and previously not described in mice.

Introduction

Plasmacytoid dendritic cells (pDCs) specialize in the production of type I interferons (IFNs) and promote antiviral immune responses following engagement of pattern recognition receptors. They have been mainly implicated in the pathogenesis of autoimmune diseases that are characterized by a type I IFN signature (notably, IFN-α). Yet, pDCs have also been shown to be able to induce tolerogenic immune responses[5-8]. Due to the clinical significance of pDCs, several studies aimed at mapping pDC lineage derivation have emerged recently. Yet, a complete understanding of pDC development and their existing subsets in mice is still lacking. The transcription factor 4 (TCF4) is required for pDC development and for lineage

identity[9-11]. TCF4 is a component of a multiprotein complex that includes both positive and negative regulators[6,12]. One of these components, the transcription factor BCL11a, which is also essential for B cell development[13-15], induces *Tcf4* transcription and initiates a positive feedback loop with TCF4 to maintain pDC lineage commitment and function[14-16].

Unlike their conventional dendritic cell (cDC) counterparts, pDCs express transcriptional regulators and markers associated with B-lymphocyte development in addition to BCL11a (e.g. B220, SPIB)[17,18]. These features, along with the established generation of pDCs from myeloid restricted precursors[58, 76], have made it difficult to define pDC lineage affiliation[11,17,19,20]. This has led to the hypothesis that pDC subsets may have distinct origins derived from either the Common Lymphoid Progenitor (CLP) or the Common Myeloid Progenitor (CMP)[18, 61]. Beyond the complex nature of their lineage, pDCs with different functional attributes (e.g. variable IFN- α expression levels) or different surface markers (e.g. $CD19^+$ pDCs detected in tumor-draining lymph nodes) have also been identified[17,21-23].

On par with the ever-increasing heterogeneity described within pDC populations, a novel AXL+ dendritic cell (DC) population with many pDC-like properties has recently been discovered in human blood[1,3,4]. While AXL+ DCs express many canonical pDC markers (e.g. CD123, BDCA2/CD303), they also express CD2, the Ig-like lectins SIGLEC1 and SIGLEC6, as well as the activation marker CD81[1]. In a separate study[2], a similar population of pDCs was shown to express high levels of CD5 and CD81 in mice and humans, two glycoproteins normally associated with the B cell receptor (BCR) signaling complex. The origin of AXL+ transitional DCs is currently unclear and the presence of a homologous population in mice remains muddled. Here, we report the identification of a

lymphoid-derived pDC subset (B-pDCs) that shares inflammatory features with myeloid derived *Axl*+ pDC populations in mice. We also demonstrate an in vivo requirement for *Bcl11a* in the transcriptional specification of B-pDCs.

Results

We previously demonstrated that conditional deletion of *Bcl11a* in the hematopoietic stem cell (HSC) compartment mediated by *Vav-1*-Cre or by inducible *Mx1*-Cre recombinase results in complete abolishment of pDC development[14]. Spurred by previous speculation of pDC origin from the CLP[17,20], we next selectively deleted floxed (^{F}) *Bcl11a* alleles in CD79a^{+} cells [24,25,] as mediated by *mb1*-Cre *in vivo*. Expression of the *mb1* gene (CD79a) initiates at the LY6D^{+} CLP stage, in B-cell-biased lymphoid progenitors (BLPs)[26], downstream of LY6D^{-} CLPs (Fig. S1). *Bcl11a$^{F/F}$mb1-Cre* mice (cKO) and littermate controls were examined for pDC frequencies among nucleated cells in the bone marrow (BM). B220^{+} PDCA1^{+} pDCs (all found to be CD11c^{int}) were consistently and significantly reduced by an average of ~25% (24.8 ± 2.4%) in cKO mice relative to littermates (Fig. 1A-B). Loss of B cells (B220^{hi} PDCA1^{-}) served as a gauge of *mb1-Cre* deletion efficiency (Fig. 1A-B). Taken together, these data indicate that a significant proportion of pDCs are derived from BLPs or BLP-derived cells and are *Bcl11a* dependent.

To expand these *in vivo* observations, and to confirm that this defect is intrinsic to hematological progenitor cells, we transferred BM from either BCL11A -sufficient reporter control mice (*mb1-Cre-YFP*) or BCL11A-deficient cKO mice (*Bcl11a$^{F/F}$mb1-Cre-YFP*) into lethally irradiated wild type C57BL/6J recipients. After 8 weeks, <10% of B cells (B220^{+} PDCA1^{-}) in the spleens of *mb1-Cre-YFP* recipients were YFP^{-}, confirming elimination of recipient hematopoiesis (Fig. 1D-E). As expected, *Bcl11a$^{F/F}$mb1-Cre-YFP*

BM resulted in significantly reduced B cell and pDC cellularity compared to *mb1-Cre-YFP* controls, whereas BCL11A-sufficient (YFP^{-}) pDCs persisted (Fig. 1C, 1E-F). Approximately 1/3 of pDCs in the spleen of wild-type chimeras were YFP^{+} compared to only 1/5 in BM (Fig. 1G). This increased fraction of YFP^{+} pDCs in the spleen suggests that BLP-derived pDCs preferentially home to that organ. While the residual YFP^{+} pDCs in the BM might be an indication that *Bcl11a* is not shut-off at the most precise developmentally-critical point within the B cell lineage for complete CD79a+ pDC ablation, other hematopoietic lineages were capable of development in normal numbers and contained a paucity of YFP^{+} cells (Fig. S2). Of note, BCL11A-deficient progenitors yielded higher splenic T cell chimerism at the expense of B cells and pDCs, but less than 2% of T cells were YFP^{+} (S2, and not shown). This indicated that *mb1-cre* expression occurs subsequent to T-B lineage divergence, consonant with previous observations[26, 68, 69] and our *mb1-cre* progenitor analysis in which YFP^{+} cells are confined to the BLP derived compartment (Fig. S1). Because of their exclusive lymphoid derivation post T-B bifurcation, we were prompted hereafter to refer to this pDC lineage as "B-pDC".

Relative to $CD79a^{-}$ pDCs, resting B-pDCs express higher levels of MHC Class II (Fig 2A-B) suggesting that they may be primed for immediate response to pro-inflammatory signals. To test this hypothesis, we delivered TLR9 ligand (CpG:ODN) into *mb1-Cre-YFP* mice via tail vein injection, and splenic pDCs were phenotyped via flow cytometry 24 hours later. While both pDC and B-pDC compartments expanded relative to controls (Fig. 2C-D), the YFP^{+} B-pDC fraction increased almost 2-fold above that of the YFP^{-} pDC fraction in numbers (Fig. 2E). Additionally, fold increase of B-pDCs coexpressing CD83 and CD86 upon activation was also significantly higher than that of YFP^{-} pDCs (Fig. 2F-G).

These results suggested that relative to YFP$^-$ pDCs, B-pDCs are intrinsically activated and primed for rapid expansion upon TLR9 engagement. To confirm the functional phenotype of B-pDCs, we tested their ability to secrete cytokines known to be elicited by pDCs after Toll-like receptor (TLR) engagement. Specifically, we tested each pDC lineage for the production of IFN-α or IL-12p40 when activated by TLR9-bound CpG oligonucleotides. We sorted B-pDCs and pDCs, engaged TLR9 with CpG:ODNs for 24 hours and collected supernatant for cytokine specific ELISAs. IFN-α production was almost negligible in B-pDC ($p<0.0001$, Fig. 2H), yet IL-12p40 production was significantly augmented over pDC ($p<0.0001$, Fig. 2H). To test their ability to expand T lymphocytes in culture, sorted B-pDCs and pDCs were incubated with CpG:ODNs and co-cultured with freshly isolated CFSE-labeled lymphocytes. After 6 days, co- cultures were stained for CD3 and CFSE-negative cell percentages were recorded (Fig. 2I-J). Altogether, our results showed B-pDCs were significantly better at expanding T cells in co- cultures than conventional pDCs ($p<0.001$, Fig. 2I-J) upon TLR9 activation.

To further elucidate their phenotype at the genetic level, we performed RNA-seq analyses of purified B-pDCs and compared them to classical, myeloid-derived bulk pDCs. Expression of hallmark pDC genes was confirmed by RT-PCR of shared pDC markers (Fig. S3A). While the overall gene expression patterns were highly similar across the two subsets, ~1% of transcripts (~220 genes) differed significantly (q value< 0.05) (Fig. S3B). Among the top overexpressed genes in B-pDCs were *Lyz1, Ccr3, Cd86, Id2, Axl, Siglec1, and Cd81* (Fig. S3C). Differentially expressed transcripts generated Gene Ontology (GO)[27] or Panther[28] terms including “immune response”, “inflammatory response”, “cell activation”, and “regulation of immune response” ($p=1.36x10^{-17}$, $2.15x10^{-12}$, $3.67x10^{-11}$, and $1.45x10^{-10}$,

respectively (Fig.S3C). Gene set enrichment analysis (GSEA) revealed elevation of each of these same GO/Panther terms within the B-pDC subset as compared to a pDC-related GSEA control dataset that showed no enrichment. Next, we compared all genes expressed by both pDC populations to one another and to published[29] RNA-seq of BM-derived mouse pre-B cells ($B220^+$ IgM^- Kit^- $CD25^+$)—a post-CLP B cell progenitor (pre-B) population. As shown in Figure S3D, pDCs and B-pDCs expression levels were strongly correlated with one another relative to early B cells (R^2 values = 0.8959, 0.4145 and 0.404, respectively) (Fig.S3D). Collectively, these data support our contention that B-pDCs are functionally distinct from classical pDCs and specialize in inflammatory responses, antigen presentation, and T cell activation.

AXL^+ transitional DCs (tDCs or AS-DCs)[1, 57] have been identified in humans by the high expression levels of the genes *AXL*, *CD81*, *CD86*, *LYZ2*, *C1QA*, *CD2*, and *C1QB* relative to classical pDCs [1-4]. They also exhibit many classical pDC features, having previously been described phenotypically as a "continuum" between pDC and cDC2 populations [2]. In order to confirm AXL^+ pDCs are also present in mice and corroborate our RNA-seq findings, we phenotyped B-pDCs through imaging flow cytometry. First, we again verified that our primary gating scheme effectively encompassed bona-fide pDCs using imaging flow cytometry. As expected, $B220^+$ $PDCA1^-$ cells were >95% $CD19^+$ SIGLEC-H^- (B cells). Most importantly,>95% of $B220^+$ PDCA1 ^{hi} cells were SIGLEC-H $^+$ and $CD19^-$, ruling out any pDC population contamination (Fig. S.4A-B). At the protein level, we were able to stain mouse BM cells with anti-AXL antibodies without issues and confirmed that while ~60% of B-pDCs were positive for AXL, only ~10% of YFP negative pDCs expressed this protein (Fig. S4A, C-E). Finally, imaging of BM cells showed that B-pDCs resembled

classical secretory pDCs morphologically, presenting a large nucleus and defined plasma-like features, in contrast to B cells (Fig. S4A). This preliminary phenotypic analysis led us to speculate that similarly to human AXL$^+$ transitional DCs, B-pDC might also prioritize their secretory capacity for copious transcription and secretion of alternative immune system modulators. Thus, we performed high resolution 10x single cell RNA-seq analyses of magnetically sorted PDCA1$^+$ bone marrow cells (96% purity as determined by flow cytometry) and compared the B-pDC transcriptional profile to that of B cells and other pDCs. Principal component-based clustering and UMAP visualization of sorted PDCA$^+$ cells yielded 22 discrete clusters. To identify cell populations in an unbiased manner, we uploaded the top 1000 differentially expressed genes (DEGs) from each cluster into CIPR (Cluster Identity Predictor)[66], which uses the reference database ImmGen (mouse) to calculate cell identity scores (S. Table 1). Seurat clusters were named according to the consensus of the top 5 cell ID hits generated by CIPR (Fig. 3A). We confirmed CIPR assignments by evaluating cluster DEGs and expression of markers associated with specific myeloid cell populations (Fig. S5). PDCA1$^+$ cells comprised 9 distinct pDC populations (including B-pDCs, which were unanimously classified as pDCs by CIPR identity scores despite its unique *Cd79a* expression). Of note, pDC8 had one of the lowest ID scores among consensus pDCs (S. Table 1) and yielded CIPR identity hits for both pDCs and common myeloid progenitors "CMPs" within its top 5 ID hits (not shown). This suggested that this single cluster (1.7% of total cells) represented a mixed population of pDCs and differentiating CMPs expressing high levels of *Hbb* family genes (hemoglobin associated genes) under the chosen default Seurat clustering resolution settings. Because of pDC8 mixed identity, we excluded this cluster from our further single cell transcriptional analysis.

Besides pDCs, a small B cell cluster (2.75% of all cells analyzed) expressing low levels of *Bst2* (PDCA1 gene), as well as distinct subpopulations of macrophages (Mac1, 2, and 3), monocytes (Mono1, 2 and 3), and granulocytes (Granul1, 2, and 3) were also identified. Two stem-progenitor populations (Prog1 and 2) were present in our cell pool (1.12% and 2.86% of cells analyzed, respectively) (Fig. 3A-B). The Prog2 population expressed high levels of genes associated with pDCs, including *Siglech*, *Bst2*, *Flt3*, *TCF4*, and *Irf8* and had a "CDC" (common dendritic cell progenitor) signature according to its CIPR reference ID (Fig. S5, S. Table 2). In addition, the majority of cells in the Prog2 cluster were *Csf1r*$^{-}$, *Il7r*$^{+}$, *Siglech*$^{+}$, *Ly6d*$^{+}$ (Fig. S5, S. Table 2), resembling the pro-pDC myeloid precursor population described by Rodriguez *et al*, as well as Dress and colleagues[70, 67]. In contrast, Prog1, which clustered near B cells and was identified as "MLP" (multi-lymphoid progenitors entering the CLP stage), expressed several pre/pro B cell genes, including *Jchain*, *Iglc1*, *Iglc2*, *Igha*, *Igkc* (S. Table 2). Direct DEG comparison between Prog1 and Prog2 clusters confirmed Prog1 cells exhibit a more "Pre/Pro B cell-like" developmental profile and low expression of markers that are "pDC biased" relative to Prog2 (S. Table 2). After clustering and profiling PDCA1^{+} cells, we subsetted the data in order to compare B-pDCs gene expression to only B cell and pDC clusters using Wilcoxon rank sum tests. We plotted several genes commonly associated with B cells, and pDCs. Except for *Cd79a (Mb1)* and *Cd79b*, B-pDCs showed negligible expression of mature B cell associated genes such as *Pax5*, *Cd19* and *Cd22* (Fig. 3C). Expression of canonical pDC genes was present but reduced in B-pDCs relative to classical pDC subsets (Fig. 3D). Our analysis highlights the B-pDC cluster uniqueness among pDC subsets and further supported its lineage divergence from mature B cells.

In order to temporally examine lymphoid transcriptional commitment to B cell or B-

pDC lineages, we inferred developmental trajectories for B and B-pDC single cells. Pseudotime is a measure of how much progress an individual cell has made through a process such as differentiation[59, 60]. In other words, cells that belong to a single cluster can be segregated across various transcriptional "states" based on number of reads per cell of a particular set of developmental genes. Although we cannot say the pre/pro B cell- like Prog1 cluster represents an immediately adjacent common progenitor for B cells and B-pDCs, we confirmed B-pDCs are not a direct precursor for B cells based on their single cell developmental trajectory. Cells in the Prog1 cluster were chosen as state "0" based on their abundant expression of lymphoid progenitor associated genes (Fig. 4A). Analysis of uniquely expressed genes showed Prog1 downregulated several multipotency markers such as *Stmn1*, *Gata2*, and *Ctla2a*, while B cells increased expression of transcription factors needed for B cell commitment (e.g., *Pax5*, *Ebf1*, and *Ms4a1*) (Fig. 4B and 4C). Although B-pDCs did not express detectable levels of most B cell commitment markers evaluated, they did retain expression of early B cell receptor associated genes, including *Ly6d*, *Ighm*, *Igkc*, *Iglc2*, and *J Chain* (Fig. S6A). Because these early B cell related markers are also expressed in plasma cells, we performed flow cytometric analysis of B220^{+} PDCA1^{+}: CD79a^{+} cells. We discovered that B-pDCs express negligible levels of TACI (a transcription factor that silences the B-cell developmental program [62]), and that expression of CD138 and IgG1 was also negligible (Fig. S6B, and not shown), thus ruling out any major plasma cell overlap at the protein level. Lineage analysis also revealed that B- pDCs enhanced expression of the pDC associated markers *Siglech*, *Tcf4*, *Bst2*, and also of *Xbp1* (a marker expressed at high levels in secretory cells). Committed B cells in turn downregulated these markers as they progressed through pseudotime (Fig. 4D). In

summary, lineage analyses revealed that as B-pDCs develop, they retain expression of both early B cell receptor genes and pDC associated genes, diverging from B cells through continued suppression of transcription factors required for terminal B cell differentiation.

In order to determine if murine B-pDCs are homologous with AXL+ human DCs, we subsetted pDCs clusters and plotted their relative expression of AXL+ DC associated genes. We identified B-pDCs and pDC5 as "noncanonical pDCs" due to their distinguishing high expression of *Axl* (Fig. 5A). Accordingly, *Axl* negative pDCs are referred hereafter as "classical pDCs". We then analyzed the top DEGs shared between B-pDCs and pDC5s using the function "FindConservedMarkers". *Lyz2*, the complement genes *C1qa, C1qb, C1qc*, and *Cd5l* were the top conserved markers for these two pDC subsets (Fig. 5A). Of note, *Cd5l*, a macrophage associated secreted protein, has been shown to play a major role in initiating inflammation and maintaining humoral responses. [71-73] Unexpectedly, the number of reads for myeloid markers previously used to define human AXL+ DCs via CyTOF or RNA- seq[1,57,67,69,70] was negligible in murine pDCs and weakly correlated with expression of *Axl* itself in mice (Fig. S7). *Cd81* expression, however, was highly expressed in B-pDCs (Fig.S7A). Of note, *Cd81* and *C1qb* have been described as hallmark genes of a discrete mouse pDC population that does not produce type I IFN and yet mediates important immune functions previously attributed to all pDCs[2, 37]. Altogether, our analysis revealed that constitutive expression of *Axl* and innate activation markers are present in more than one transcriptionally distinct murine pDC profile, stressing the functional heterogeneity and plasticity of murine pDCs.

Noncanonical AXL+ DCs in humans have been shown to be derived from a myeloid pro-pDC progenitor[67,69,70]. In mice, Feng and colleagues used clonal lineage to show that

pDCs and cDCs originate from a common Flt3-dependent pathway of differentiation originating from transient CX3CR1^{+} progenitors. Since the authors state that their finding does "not completely rule out the common origin of pDCs and B cells, which may bifurcate earlier in hematopoiesis", we set out to corroborate the hematopoietic origins of pDC5 and B-pDCs. We first calculated pDC5's "community connectedness" [74] to other pDC clusters and plotted their developmental trajectories originating from the pro-pDC progenitor cluster Prog2 using Monocle3[75]. Partitioning Prog2 and pDC single cells into Louvain communities yielded 5 supergroups, with the largest group encompassing most pDC clusters, including pDC5. The other groups consisted of non pDCs (Prog2 cells), B-pDCs, and a few single cells (>20 cells) genotypically distinct from their original pDC clusters (Fig. 5B). Ultimately, this statistical grouping confirmed that B-pDCs were not developmentally linked to "classical" AXL negative pDCs or *Axl*+ pDC5 cells. Accordingly, B-pDCs did not integrate into the predicted lineage trajectory originating from Prog2, whereas the *Axl*+ pDC5 population did (Fig. 5B). Both B-pDCs and pDC5s exhibited a similar late developmental pseudotime, while clusters pDC6 and pDC4 were the first to develop from Prog2. Collectively, our data establish that murine non canonical pDCs (AXL+) consist of at least two major pDC subpopulations, which develop from lymphoid and myeloid progenitors, respectively.

Discussion

Dendritic cell–subset biology, development, and the ensuing nomenclature have long been unclear and everchanging. Here, we provide definitive evidence in support of the long- suspected "lymphoid past" of pDCs by establishing their ability to arise *in vivo* from CLP derived progenitors with B/pDC bipotential lineage capacity[17-19,43,44]. Our data shows

that the murine pDC compartment is bipartite, being comprised of B-pDCs—diverted from the CLP post T-B bifurcation—as well as myeloid-derived classical pDCs. Unlike most myeloid derived pDCs, B- pDCs constitutively express high levels of multiple innate activation markers, including *C1qa, C1qb, Lyz2, and Cd81*. Functionally, they expand more readily after TLR9 engagement than classical pDCs and excel at activating T cells in culture. While further functional definition awaits discovery, our work provides a framework for the identification and segregation of the B-pDC lineage (comprising almost 1/5 of the total pDC compartment) from other myeloid- derived pDC subpopulations. Primarily, our observations support the hypothesis that DC functionality derives primarily from ontogeny rather than from tissue environment [50], exemplified by evolution of a specialized pDC lineage from a lymphoid progenitor. In the case of the B-pDCs, our data suggest such a cell may deviate from B cell commitment after *Ly6d* expression, thought to be the earliest marker of B cell specification[26].

Most noticeably, our newly described B-pDC population expresses high levels of the tyrosine kinase AXL and specializes in T cell activation through displaying high levels of MHC II and costimulatory markers. Of note, ablation of AXL in mice has previously been shown to increase expression of type I IFN while impairing IL-1β production and T cell activation during viral infections. [63, 64] Our related findings that AXL+ B-pDCs excel at T cell priming but exhibit reduced IFNα expression might suggest these DCs play an important role advancing T cell expansion, while curbing innate immune responses that can result in autoimmune damage. In addition to describing a novel B cell-like pDC population, we profiled murine pDCs, and established that murine AXL^+ pDCs can develop in parallel from either myeloid or lymphoid progenitors, with lymphoid derived B-pDCs retaining

expression of additional early B cell genes that are not expressed in myeloid derived pDCs. Intriguingly, ChIP-seq analysis done by our lab of BCL11A target binding in multiple human cell lines suggests that an evolutionarily conserved transcriptional hierarchy might distinguish AXL^{+} pDCs and B cells in humans as well (unpublished data). The demarcation of lymphoid derived B- pDCs as one of the AXL^{+} pDC populations found in mice may help clarify the perceived plasticity of the pDC compartment in normal and disease contexts[51], as well as provide a new cell for targeted study within the context of autoimmune disease, cancer, and infection models.

Figure Legends

Figure 1. Mb1-Cre deletion of *Bcl11a* identifies a CLP-derived subset of pDCs

(A) Representative FACS plots of pDC (gated as B220^{+} PDCA1^{+}) and B cell (gated as B220^{+} PDCA1-) percentages in the bone marrow (BM) of *Bcl11a* $^{F/F}$ *mb1*-Cre mice (cKO) and littermate controls. (B) Quantification of pDC and B cell populations in the BM of *Bcl11a* $^{F/F}$ *mb1*-Cre mice (cKO) and littermate controls as cells/100,000 cells. (C-D) Flow cytometric analysis of BM and spleens of recipient mice 8 weeks post BM transplantation. BM was transferred from either BCL11A -sufficient reporter control mice (*mb1*-Cre-YFP) or BCL11A- deficient cKO mice (*Bcl11a* $^{F/F}$ *mb1*-Cre-YFP) into lethally irradiated C57BL/6J recipients. (E) B cell numbers after BM transplantation in BM and spleens of recipient mice. (F) pDC numbers after BM transplantation in BM and spleens of recipient mice. (G) Comparison of YFP^{+} pDC percentages in the spleen and BM of recipient mice post BM transplantation. Student's t-test was used for all statistical comparisons. Error bars=mean±s.d. The results are representative of two experiments each containing 3-4 mice per group.

Figure 2. CLP-derived B-pDC are licensed for T cell activation

(A-B) Comparison of MHCII MFI in YFP^+ and YFP^- pDCs from *Mb1*-Cre-YFP reporter mice via flow cytometric analysis. ***p=0.0005 (C-D) *Mb1*-Cre-YFP mice were injected with 50 ug/ml (100 ul) of CpG:ODN or control GpC:ODN and analyzed via flow cytometry for splenic pDC numbers/100,000 cells (***p<0.0001). (E) Flow cytometry quantification of YFP^- pDC and B- pDCs (YFP^+) fold change in cell numbers upon CpG:ODN in vivo challenge (**p=0.002142 for YFP negative pDC expansion; ***p= 0.00023 for B- pDC expansion, and *p=0.0151 for CpG stimulated B-pDC and YFP^- pDC number comparison). (F-G) Fold change in $CD86^+CD89^+$ cell numbers for each pDC population in mice restimulated with CpG:ODN; (B-pDCs , ***p<0.0001; YFP^- pDCs, **p=0.026). Difference in $CD86^+CD89^+$ cell numbers between stimulated B-pDCs and YFP^- pDCs was also significant, **p=0.0034 (H) In vitro TLR9 engagement of B-pDC or pDC for ELISA against IFN-α orIL-12p40. (****p<0.0001 for both cytokines) (I) T cells were magnetically isolated from wildtype C57BL/6J mouse splenocytes using MACs columns, labelled with CSFE, and then cultured ($2.5x10^4$/well) alone or with CpG:ODN activated B- pDCs or pDCs ($5x10^3$/well) for 6 d. (J) The percentage of CFSE-negative $CD3^+$ T cells in co- cultures were significantly higher in B-pDC compared to pDC (****p<0.0001). Student's t-test was used for all statistical comparisons. Error bars=mean±s.d. The results are representative of three independent experiments each containing at least four mice per group.

Figure 3. Single cell RNA-seq analysis of mouse $PDCA1^+$ bone marrow cells

(A) UMAP generated by Seurat clustering analysis. Cluster identities were assigned using the top 5 consensus CIPR identity scores. (B) Heatmap of the top 5 DEGs from each cluster. After Seurat clustering, cell reads were subsetted to include only cells classified as B cells,

pDCs, and B- pDCs. DEGS were generated for the new data subset and markers associated with (C) mature B cells (D) classical pDCs were plotted as violin plots.

Figure 4. Single cell trajectory analysis of Prog1, B cells, and B-pDC clusters

(A) Single cells belonging to clusters Prog1, B cells, and B-pDCs were ordered and plotted as a function of pseudotime based on uniquely expressed markers using the unsurpevised Monocle dpFeature. Cluster Prog1 was classified as the root of the trajectory given its high expression of pre-pro B cell and stem cell associated markers. DEGs of interest were plotted as a function of pseudotime in Prog1 (B), B cells (C), or pDCs (D) using Monocle. Branch Y_112 represents the expression kinetic trend of the B-pDC cluster (green), while branch Y_83 represents the expression kinetic trend in expression of B cells according to branched expression analysis modeling, or BEAM.

Figure 5. Identification of Axl$^+$ non-canonical pDCs in mice

(A) Violin plots depicting relative expression of conserved "non canonical *AXL*$^+$ DCs" associated markers in mouse pDC clusters. (B) BM scRNA-seq data was subsetted to include only pDCs and Prog2 subsets. We used Monocle3 for partition-based learning of cell developmental trajectories. Louvain partitions were generated from single cell reads and their developmental trajectory was inferred using SimplePPT (top right quadrant). Pseudotime across clusters is shown in the (lower bottom quadrant).

Supplemental Figure Legends

Supplemental Figure 1. Progenitor population analysis for mb1-cre driven YFP expression. We analyzed YFP expression in BM progenitors to determine when and where mb1-Cre is active (representative plots shown). (A) Lineage negative cells were analyzed to

examine LSK Hematopoietic progenitor (Lin$^-$, Sca-1$^+$, c-Kit$^+$), MPP (LSK, Flt3^{int}), and LMPP (LSK, Flt3^{hi}), populations. Virtually all cells were YFP$^-$. (B) Myeloid Dendritic Progenitors (MDP; Lin$^-$, IL7Rα^-, Flt3$^+$, c-kit^{hi}, Sca1$^-$) and (C) Common Dendritic Cell Progenitors (CDP; Lin-, IL7Ra-, Flt3$^+$, c- kitlo, Sca1-, CD115$^+$) were also negative for YFP expression, while (D) Common Lymphoid Progenitors (CLP; Lin$^-$, IL7Ra$^+$, Flt3$^+$, c- kit^{lo}, Sca1^{lo}) contained YFP$^+$ cells. Error bars=mean±s.d. The results are representative of three independent experiments each containing at least three mice per group.

Supplemental Figure 2. Cell distributions in the spleen of adoptively transferred recipient mice. Both *Bcl11a* $^{F/F}$ *mb1*-Cre$^+$ and *Mb1*-Cre-YFP adoptively transferred recipient mice reconstituted other splenic cell types in normal numbers, including BM macrophages (CD11b$^+$ F4/80$^+$), granulocytes (Gr-1$^+$ CD11b$^+$) and splenic cDCs (CD11c$^+$ CD11b$^+$ B220$^-$). Total T cells (CD3$^+$ B220$^-$) as well as CD4$^+$ and CD8$^+$ subsets were significantly increased in number in proportion to B/pDC cell loss. Student's t-test was used for all statistical comparisons. The results are representative of two independent experiments each containing 3-4 mice per experimental group. Error bars=mean±s.d

Supplemental Figure 3. Transcriptional analysis identifies two populations of pDC in mice: myeloid-derived classical pDC and CLP-derived B-pDC. (A) Bone marrow pDC (B220$^+$ PDCA1$^+$ CD11c^{int} CD11b$^-$) were sorted based on expression of YFP. Four mice were pooled for each isolated RNA sample, for a total of three pDC and three B-pDC groups from 12 mice. RT-PCR was used to confirm that *Bcl11a, Bst2, SpiC, and Id2* expression match RNA- seq trends between pDC and B-pDC (B) RNA-seq was performed for gene expression analysis of pDC vs B-pDC and 220/23,946 genes (~1%, left) were significantly differentially expressed (q value < 0.05, right heatmap, Log2 expression difference displayed). (C) Gene

Set Enrichment Analysis (GSEA). Normalized enrichment score (NES) and false discovery rate q- values(FDR);FDR≤.25isconsideredsignificant[56]. GO Term or Panther- derived pathways identified by DAVID analysis of ~220 differentially expressed genes between the pDC and B- pDC subsets[28,29.] Among the top B-pDC DEGs were *Lyz1, Ccr3, Cd86, Cd83, Id2, Axl, Siglec1, and Cd81*. (D) Scatter plot comparisons of all genes with Reads Per Kilobase of transcript, per Million mapped reads (RPKM) >1. Correlations of pDC vs B-pDC (R2 value = 0.8959), B cell vs. pDC R2 value = 0.4145) and B cell vs. B-pDC (R2 value = 0.404) are indicated.

Supplemental Figure 4. Imaging flow cytometry as a tool to quantify AXL expression in pDC populations. (A-B) Representative Imaging flow cytometry of manuscript gating scheme used to define B cells and pDCs and histograms for SIGLEC-H, AXL and CD19 in B cells and pDCs (C) Representative Imaging flow cytometry plots of AXL^+ pDCs (here alternatively gated as SIGLEC-H^+ $PDCA1^+$) in *Mb1*-Cre-YFP reporter mice bone marrow cells (n=5). (D) Complete statistics table generated with IDEAS for Image Stream analysis including non-stained wildtype controls. (E) Comparison of AXL expression in YFP^- and YFP^+ (B-pDCs) ($p<0.0001$, unpaired t tests). The results are representative of two independent experiments each containing at least 3 mice per group.

Supplemental Figure 5. Confirmation of unbiasedly identified cell cluster identities. Seurat generated violin plots of genes associated with distinct cell populations including mature B cells, pDCs, granulocytes, pre-pDCs, NK cells, monocytes, macrophages, and myeloid progenitor cells. Plot identities were initially determined by running the package CIPR (Cluster Identity Predictor).

Supplemental Figure 6. Expression of early B cell receptor genes in B-pDCs. (A)

Monocle was used to plot select early B cell genes as function of branched pseudotime for Prog1, B Cells, and B-pDC populations. (B) Plasma cell contamination in *Mb1*$^{+}$ pDCs (B220^{+} PDCA1^{+}) was ruled out by flow cytometric analysis of TACI and CD138 in BM of 6 C57BL/6J mice.

Supplemental Figure 7: Transcriptional heterogeneity of *Axl*$^{+}$ murine pDC populations. (A) Dot plot depicting expression prevalence of select "*AXL*$^{+}$ DC" associated markers from literature select and pDC DEGs for pDC subsets. (B) Correlation between expression of AXL+ DC associated markers and *Axl* in non-canonical mouse pDC subsets.

Supplemental Table 1. Top CIPR Assigned Identity Scores for Seurat Cluster DEGs. CIPR IDs were generated using the top 1000 DEGS from each cluster. The top 5 consensus CIPR ID generated was used to rename Seurat clusters.

Supplemental Table 2. DEG comparison between progenitor clusters.

The top 50 differentially expressed features of Prog1 in relation to Prog2 were calculated using Seurat using non-parametric Wilcoxon rank sum test. In blue are upregulated genes and in red are downregulated genes.

Methods

Mice

Generation of *Bcl11a* cKO Mice (C57BL/6J background) was performed as described[14]. To generate conditional knockouts for the *Mb1* gene, specifically, *Bcl11a* $^{F/F}$ mice were crossed to *Mb1*-Cre^{+} Rosa26-YFP^{+} reporter mice. *Mb1*-Cre deleter and Rosa26- YFP

reporter strains (C57BL/6J genetic background) were obtained from Jackson labs (catalog #'s 020505 and 006148, respectively), bred, and genotyped according to the vendor protocol and their validated primers). All housing, husbandry, and experimental procedures with mice were approved by the Institutional Animal Care and Use Committees at the University of Texas at Austin. 6-week-old gender matched male or female mice were used for all experiments described in this manuscript. For each experiment, at least 4 samples per experimental group were used, with each experiment repeated at least 3 times (except for bone marrow reconstitutions and imaging flow cytometry experiments, which were repeated twice).

Tissue processing

Mouse femurs were cut at the extremities and a 25G needle was inserted in the bones to flush out bone marrow cells with 10 ml of cold PBS onto a 70 uM strainer in a 50 mL tube. Cells were washed from the strainers into the tubes with an additional 10 mL of PBS. Tubes were spun at 300G for 5 minutes and supernatant was decanted. 2 mL of ACK red blood cell lysis buffer was used to resuspend cells, which were incubated for 2 minutes and 20 seconds. Samples were diluted with 20 mL of cold PBS, washed once, re-filtered and resuspended in 200 uL of FACS buffer for subsequential flow cytometry staining. Spleens were mashed onto pre- wet 70 uM filters in a 50 mL tube with syringe plungers and 20 mL of cold PBS was added through the strainers into the tube. Cells were spun at 300G for 5 minutes and supernatant was decanted. 2 mL of ACK red blood cell lysis buffer was used to resuspend cells, which were incubated for 2 minutes and 20 seconds. Samples were diluted with 20 mL of cold PBS, washed once, re-filtered and resuspended in 200 uL of FACS buffer for subsequential flow cytometry staining.

Flow cytometry

Single cell suspensions ($1x10^6$ cells) were resuspended in 200 uL of FACS buffer (5mM EDTA and 1% Heat Inactivated Fetal Calf Serum in D-PBS) and incubated for 15 minutes with surface antibody cocktail (each antibody at a concentration of 1.25 micrograms/ml in FACS buffer) in the dark at 4C. Cells were then washed 3 times with FACS buffer and ran live on a BD LSRII Fortessa. Single color controls for panel compensation were made using AbC Total Antibody Compensation Bead kit (ThermoFisher Scientific), by staining each control with one of the panel antibodies and using these controls to compensate the flow cytometer experiment prior to running the samples. A non-stained sample of cells was included in experimental runs and used to adjust for autofluorescence and any nonspecific staining. FMO single cell controls were also included in some of the experimental runs (cells stained with all antibodies in the panel minus one), for compensation quality control and to detect positive MFI thresholds for each fluorophore using cells. Sorting was performed on a FACS Aria (BD Biosciences). All analysis was done using FlowJo (Tree Star) software. Single-cell suspensions were stained with the following antigen-specific monoclonal antibodies (clones in parenthesis): anti CD45R/B220-BV605 (RA3- 6B2), CD19-Alexa Fluor 700 (6D5), CD86-APC-Cy7 (GL-1), I- A/I-E-Pacific Blue (M5/114.15.2) , IL7R-BV421 (A7R34), cKit-PE-Cy7 (ACK2), CD11b- PerCP-Cy5.5 (M1/70), CD3e-PerCP-Cy5.5 (500A2), Gr1-PerCP-Cy5.5 (RB6-8C5), CD4-PerCP-Cy5.5 (RM4-5), CD8- PerCpCy5.5(53-6.7), NK1.1-PerCp- Cy5.5 (PK136), Sca1- BV711 (D7), CD135-APC (A2F10) , CD150-BV605 (TC15-12F12.2), CD79a-FITC (24C2.5) (Invitrogen), Anti-CD11c-PerCP-Cy5.5 (N418) (eBioscience), Anti-AXL-APC (175128)(R&D Systems), Anti-CD23 BV510 (B3B4)

(Biolegend), Anti-CD267-BV421 (8F10) (BD Biosciences), Anti-CD138-APC (281-2) (Biolegend), Anti-CD83-PeCy7 (Michel-19), and Anti-PDCA1-PE or Biotin (JF05-1C2.4.1) (Miltenyi Biotech), in D-PBS/2% (vol/vol) FBS FACS buffer. In some experiments, viability stain Ghost Dye Red 780 (Fisher Scientific) was used to stain cells in PBS prior to antibody staining according to the manufacturer 's protocol. Flow cytometry data was analyzed with FlowJo, while Imaging flow cytometry was performed on ImageStream X and analyzed on IDEAS® 6.0 (Amnis), by pre-filtering out of focus cells and performing automatic software guided compensation with single color controls.

Bone Marrow Transplantation

Bone marrow from 6-week-old *Bcl11a*$^{F/F}$/mb1-Cre $^{+}$ cKO or Mb-1-Cre-YFP reporter mice (n=3 per group) were collected from femurs and 5x10^6 bone marrow cells were transferred via retro-orbital injection into recipient immunocompetent C57BL/6J mice lethally irradiated with two doses of 450 rad 1 hour apart. Mice were kept on an antibiotic diet for 3 weeks to allow for immune reconstitution. Eight weeks post transfer, mice were sacrificed and cells collected from BM and spleen to investigate reconstitution of cellular subsets.

RNA isolation and RNA-seq

For sorting prior to RNA collection, BM from 12 mice was prepared from femurs at 6 weeks of age, combined into three groups (4 mice/group). Total RNA was extracted from FACS sorted *Bcl11a* cKO BM pDCs (approximately 100K YFP^{+} pDCs and 400K YFP^{-} pDCs per pooled sample) using TRIzol reagent (Invitrogen). Taq polymerase (New England Biolabs) and a Perkin-Elmer 2700 thermocycler were used to amplify transcripts for the following mouse genes: *Bcl11a* (F: 5'-GTGGATAAGCCGCCTTCCCCTT-3', R: 5'-

GGGGACTTCCGTGTTCACTTTC-3'), *Bst2* (F:5'- AGGCAAACTCCTGCAACCTG-3', R: 5'- ACCTGCACTGTGCTAGAAGTC- 3'), *SpiC* (F: 5'-ATCCTCACGTCAGAGGCAAC-3',

R: 5'-TGTACGGATTGGTGGAAGCC-3', *Id2* (F: 5'-GGACATCAGCATCCTGTCCTTGC- 3' R: 5'- GTGTTCTCCTGGTGAAATGGCTGA-3',and *β-actin* (F:5'AGGTGTGATGGTGGGAAT-3', R: 5'-GGTGTAAAACGCAGCTCAGT-3') and

probe RNA sequencing potential. For bulk RNA-seq, twelve mice were pooled into three YFP^+ groups, and total RNA was extracted as above. Oligo-dT-primed cDNA was prepared using SuperScript III First-Strand Synthesis System for RT-PCR (Invitrogen). Poly(A) mRNA was enriched using the NEBNext magnetic isolation module (E7490) and samples underwent DNAse treatment. cDNA was prepared using the Ultra Low kit from Clontech (Mountain View, CA). Libraries were prepared at the according to manufacturer's instructions for the NEBNext Ultra II Direction RNA kit (NEB, product number E7760). The resulting libraries tagged with unique dual indices were checked for size and quality using the Agilent High Sensitivity DNA Kit (Agilent). Library concentrations were measured using the KAPA SYBR Fast qPCR kit and loaded for sequencing on the Illumina NovaSeq 6000 instrument (paired- end 2X150, or single-end, 100 cycles; 30x10^6 reads/sample). Data were analyzed using a high-throughput next-generation sequencing analysis pipeline: FASTQ files were aligned to the mouse genome (mm9, NCBI Build 37) using TopHat2[53]. Gene expression profiles for the individual samples were calculated with Cufflinks54 as RPKM values. YFP^+ pDC samples were normalized to each control YFP-pDC sample. GO terms identified as significantly different: GO:0006955, GO:0009611,

GO:0048584, GO:0006954, GO:0002684, GO:0001775, GO:0009986. Panther terms: BP00148, BP00155, BP00102, BP00120. Gene Set Enrichment Analysis (GSEA) using ordered gene expression levels of Common Lymphoid Progenitor-derived B-pDC and Common Myeloid Progenitor-derived pDC were significantly enriched in both GO terms and Panther-derived gene sets. A randomly selected control GSEA curated set, GSE7831: UNSTIM_VS_ INFLUENZA_STIM_ PDC_4H_DN (defined as genes down-regulated in untreated pDC versus influenza virus infected pDC 55 showed insignificant enrichment. Normalized enrichment score (NES) and false discovery rate q-values (FDR); FDR ≤ 0.25 is considered significant[56].

TLR9 engagement

Mb1-cre-YFP reporter mice were injected via tail veins with 100ul of PBS containing 50ug of CpG:ODN (n=4) or GpC:ODN control (n=4) (CpG-B no.1826, TCCAT GACG TTCCT GACGTT; control non-CpG-B no.2138, TCCATGAGCTTCCTGAGCTT, Invivogen, USA). At 24 hours, mice were sacrificed and bone marrow and spleens were collected for pDC phenotyping.

Cell co-cultures

Mb1-YFP$^+$ B-pDC (B220$^+$ PDCA1$^+$YFP$^+$) and Mb1-YFP$^-$ pDCs (B220$^+$PDCA1$^+$YFP$^-$) subsets were sorted on a FACS Aria (BD Biosciences) by and cultured in 96-well round bottom plates (n=3 wells in triplicates, repeated twice) with RPMI medium 1640 containing 10% (vol/vol) FBS, 2 mM L-glutamine, 100 units/mL penicillin and streptomycin, 1 mM sodium pyruvate, and 10 mM Hepes, and with or without 5 μg/ml class A CpGs (ODN 1585, InvivoGen) for 24 hours. pDCs were then washed three times to remove residual CpG. Preactivated pDCs (5×10^3) were cultured with lymphocytes (2.5×10^4) magnetically sorted

from mouse spleen single cell preparations using MACs columns and the EasySep™ Mouse T Cell Isolation Kit (StemCell Technologies Cat# 19851) for a total of 6d with 20 units/mL of IL-2. CSFE labelling of lymphocytes (for which sorting purity was determined to be 97% via flow cytometry) prior to coculturing experiment was done using the CellTrace™ CFSE Cell Proliferation Kit (ThermoFisher Scientific; Cat# C34554) accordingly the manufacturer's protocol.

Enzyme-linked immunosorbent assays (ELISA).

Sorted B-pDC and pDCs (5×10^3 sorted cells per well, n= 3 per group, done in duplicate wells for each condition) were stimulated with 5 uM CpG-A (ODN 1585, Invivogen) or CpG-C (ODN 2395, Invivogen); or left untreated for 24 hs. ELISAs for IFN-α (Invitrogen) or IL-12p40 (BioLegend), respectively, was performed in 100 uL of cell free supernatants according to manufacturer's instructions. Data was acquired using a Bio-Tek model EL311 automated microplate reader measuring absorbance at 450 nm.

Statistical analysis

All flow cytometry or ELISA data were analyzed with Prism (Version 8; GraphPad, La Jolla, CA) using Student's t-test. All bar graphs show means and standard deviation (SD) and are representative of repeated experiments. These data were considered statistically significant when p-values were <0.05.

10x Single cell RNA-seq analysis

PDCA1$^+$ C57BL/6J bone marrow cells from 4 pooled 6 week old wildtype C57BL/6J mice were magnetically sorted using MACS columns into culture medium, washed once with PBS $^+$ 0.04% BSA, and re-suspended in 32 µl PBS $^+$ 0.04% BSA. Single cell suspensions (50,000) were processed in the University of Texas Genomic Sequencing and Analysis

Facility (GSAF). Cell suspensions were loaded on the Chromium Controller (10X Genomics) and processed for cDNA library generation following the manufacturer's instructions for the Chromium NextGEM Single Cell 3' Reagent Kit v3.1 (10X Genomics). The resulting libraries were examined for size and quality using the Bioanalyzer High Sensitivity DNA Kit (Agilent) and their concentrations were measured using the KAPA SYBR Fast qPCR kit (Roche). Samples were sequenced on the NovaSeq 6000 instrument (paired end, read 1: 28 cycles, read 2: 90 cycles) with a targeted depth of 71,130 reads/cell. Cellranger (v3.0.2) was used to demultiplex samples, to map data to the mouse transcriptome (mm10) and quantify genes. The gene counts matrix was read into Seurat (v3.2.1). Cells with unique feature counts over 3,500 or less than 200, and >3% mitochondrial read counts were removed from the analysis. The data was normalized and transformed using scTransform. Cells were clustered based on the top 1000 variable features, 20 PCs, and a resolution of 0.6 (Seurat's graph-based clustering approach), and then visualized using UMAP. Analysis of the normalized and filtered single cell gene expression data (median of 16,181 genes across 13,838 single-cell transcriptomes) was used for the final expression table and downstream analysis. Wilcoxon rank sum test was used to test for differential expression among clusters and identify gene markers (logfc.threshold = -1 , min.pct= 0.25). Gene markers and other genes of interest were visualized using violin plots, dot plots, and heatmap plots. Unsupervised ordering of PDCA1^{+} cells was done with the Seurat integrated results as input to build a tree-like differentiation trajectory using the DDRTree algorithm of the R package Monocle v2 [59]. Select DEGs of B-pDCs, B Cells, and Prog1 populations were set as ordering genes for each trajectory, with the root state set as Prog1 classified cells. Expression of genes as a function of pseudotime was plotted with the

plot_genes_branched_pseudotime Monocle function. We also used Monocle3 to generate partition-based learning of single cell developmental trajectories with SimplePPT and plot UMAP based pseudotime figures with initial reclustering parameters num_dim=60, resolution=1e-5.

Data Deposition

RNA-seq: GSE105827; ChIP-seq: GSE99019; 10x ScRNA-seq: GSE225768. Accession numbers to previously published data sets: GSE52868 (pre-B RNA-seq); GSE55043 (CAL1 ChIP-seq); ENCODE BCL11A ChIP-seq in GM1287838.

Author contributions

J.D.D. and G.C.I. designed research; A.A., J.D.D., K.G., C.R., Z.H., B-K.L., and G.C.I. performed research; J.D.D., J.L. V.R.I, L.I.E., S.Y., G.G., A.A., and G.C.I., contributed new reagents/analytic tools; A.A., J.D.D., C.R., B.-K.L., S.Z., D.O.H., and G.C.I., analyzed data and A.A. and J.D.D. wrote the paper. The authors declare no conflict of interest.

Acknowledgements

We thank June V. Harriss for expert assistance in the generation of *Bcl11a* conditional knockout mice, and Chhaya Das and Maya Ghosh for help in ChIP experiments and cell culture. The CAL1 cell line was kindly provided by Drs. Takahiro Maeda and Boris Reizis. Library preparation and Illumina ChIP- and RNA-seq were performed at the NGS core of the MD Anderson Cancer Center. Single Cell RNA-seq was performed at the University of Texas Genomic Sequencing and Analysis Facility with the help of Holly Stevenson and Dhivya Arasappan. The Lymphoma Research Foundation Fellowship 300463 (to J.D.D.);

NIH grant F32CA110624 and Owens Medical Research Foundation grant (to G.C.I.); NIH grant R35GM133658 (to S.Y.); NIH grant R01AI104870 (to L.I.R.E.); NIH grant R01CA130075 (to V.R.I.); NIH Grant R01CA31534; Cancer Prevention Research Institute of Texas (CPRIT) Grant RP120348 to the MD Anderson NGS core and CPRIT RP120459 and the Marie Betzner Morrow Centennial Endowment (to H.O.T.) provided support for this work.

References

1 Villani, A. C. et al. Single-cell RNA-seq reveals new types of human blood dendritic cells, monocytes, and progenitors. Science 356, doi:10.1126/science.aah4573 (2017).

2 Zhang, H. et al. A distinct subset of plasmacytoid dendritic cells induces activation and differentiation of B and T lymphocytes. Proceedings of the National Academy of Sciences of the United States of America 114, 1988-1993, doi:10.1073/pnas.1610630114 (2017).

3 Alcantara-Hernandez, M. et al. High-Dimensional Phenotypic Mapping of Human Dendritic Cells Reveals Interindividual Variation and Tissue Specialization. Immunity 47,1037-1050.e1036, doi:10.1016/j.immuni.2017.11.001 (2017).

4 Matsui, T. et al. CD2 distinguishes two subsets of human plasmacytoid dendritic cells with distinct phenotype and functions. J Immunol 182, 6815-6823, doi:10.4049/jimmunol.0802008 (2009).

5 Di Domizio, J. & Cao, W. Fueling Autoimmunity: Type I Interferon in Autoimmune Diseases. Expert review of clinical immunology 9, 10.1586/eci.1512.1106, doi:10.1586/eci.12.106 (2013).

6 Swiecki, M. & Colonna, M. The multifaceted biology of plasmacytoid dendritic cells. Nat Rev Immunol 15, 471-485, doi:10.1038/nri3865 (2015).

7 Sisirak, V. et al. Genetic evidence for the role of plasmacytoid dendritic cells in systemic lupus erythematosus. J Exp Med 211, 1969-1976, doi:10.1084/jem.20132522 (2014).

8 Ronnblom, L. & Pascual, V. The innate immune system in SLE: type I interferons and dendritic cells. Lupus 17, 394-399, doi:10.1177/0961203308090020 (2008).

9 Cisse, B. et al. Transcription factor E2-2 is an essential and specific regulator of plasmacytoid dendritic cell development. Cell 135, 37-48 (2008).

10 Ghosh, H. S., Cisse, B., Bunin, A., Lewis, K. L. & Reizis, B. Continuous expression of the transcription factor e2-2 maintains the cell fate of mature plasmacytoid

dendritic cells. Immunity 33, 905-916, doi:S1074-7613(10)00453-X [pii] 10.1016/j.immuni.2010.11.023 (2010).

11 Reizis, B., Bunin, A., Ghosh, H. S., Lewis, K. L. & Sisirak, V. Plasmacytoid dendritic cells: recent progress and open questions. Annu Rev Immunol 29, 163- 183, doi:10.1146/annurev-immunol-031210-101345 (2011).

12 Grajkowska, L. T. et al. Isoform-Specific Expression and Feedback Regulation of E Protein TCF4 Control Dendritic Cell Lineage Specification. Immunity 46, 65- 77, doi:10.1016/j.immuni.2016.11.006 (2017).

13 Liu, P. et al. BCL11A is essential for normal lymphoid development. Nat Immunol 4, 525-532 (2003).

14 Ippolito, G. C. et al. Dendritic cell fate is determined by BCL11A. Proceedings of the National Academy of Sciences of the United States of America 111, E998-1006, doi:1319228111 [pii] 10.1073/pnas.1319228111 [doi] (2014).

15 Yu, Y. et al. BCL11A is essential for lymphoid development and negatively regulates p53. J Exp Med 209, 2467-2483, doi:10.1084/jem.20121846 (2012)

16 Wu, X. et al. BCL11A controls Flt3 expression in early hematopoietic progenitors and is required for pDC development in vivo. PLoS One 8, e64800, doi:10.1371/journal.pone.0064800 (2013).

17 Pelayo, R. et al. Derivation of 2 categories of plasmacytoid dendritic cells in murine bone marrow. Blood 105, 4407-4415, doi:10.1182/blood-2004-07-2529 (2005).

18 Sathe, P., Vremec, D., Wu, L., Corcoran, L. & Shortman, K. Convergent differentiation: myeloid and lymphoid pathways to murine plasmacytoid dendritic cells. Blood 121, 11- 19, doi:10.1182/blood-2012-02-413336 (2013).

19 Shigematsu, H. et al. Plasmacytoid dendritic cells activate lymphoid-specific genetic programs irrespective of their cellular origin. Immunity 21, 43-53, doi:10.1016/j.immuni.2004.06.011 S1074761304001712 [pii] (2004).

20 Wang, Y. H. & Liu, Y. J. Mysterious origin of plasmacytoid dendritic cell precursors. Immunity 21, 1-2, doi:10.1016/j.immuni.2004.07.003

S107476130400175X [pii] (2004).

21 Yang, G. X. et al. Plasmacytoid dendritic cells of different origins have distinct characteristics and function: studies of lymphoid progenitors versus myeloid progenitors. J Immunol 175, 7281-7287 (2005).

22 Mellor, A. L. et al. Cutting edge: CpG oligonucleotides induce splenic $CD19^{+}$ dendritic cells to acquire potent indoleamine 2,3-dioxygenase-dependent T cell regulatory functions via IFN Type 1 signaling. J Immunol 175, 5601-5605 (2005).

23 Munn, D. H. et al. Expression of indoleamine 2,3-dioxygenase by plasmacytoid dendritic cells in tumor-draining lymph nodes. J Clin Invest 114, 280-290, doi:10.1172/jci21583 (2004).

24 Hobeika, E. et al. Testing gene function early in the B cell lineage in mb1-cre mice. Proceedings of the National Academy of Sciences of the United States of America 103, 13789-13794, doi:10.1073/pnas.0605944103 (2006).

25 Sakaguchi, N., Kashiwamura, S., Kimoto, M., Thalmann, P. & Melchers, F. B lymphocyte lineage-restricted expression of mb-1, a gene with CD3-like structural properties. The EMBO journal 7, 3457-3464 (1988).

26 Inlay, M. A. et al. Ly6d marks the earliest stage of B-cell specification and identifies the branchpoint between B-cell and T-cell development. Genes & Development 23, 2376-2381, doi:10.1101/gad.1836009 (2009).

27 Huang, D. W., Sherman, B. T. & Lempicki, R. A. Bioinformatics enrichment tools: paths toward the comprehensive functional analysis of large gene lists. Nucleic Acids Res 37, 1-13, doi:10.1093/nar/gkn923 (2009).

28 Thomas, P. D. et al. PANTHER: a library of protein families and subfamilies indexed by function. Genome research 13, 2129-2141, doi:10.1101/gr.772403 (2003).

29 Liu, G. J. et al. Pax5 loss imposes a reversible differentiation block in B-progenitor acute lymphoblastic leukemia. Genes Dev 28, 1337-1350, doi:10.1101/gad.240416.114 (2014).

30 Greenwald, R. J., Freeman, G. J. & Sharpe, A. H. The B7 family revisited. Annual

Rev Immunol 23, 515-548, doi:10.1146/annurev.immunol. 23.021704.115611(2005).

31 Seth, S. et al. CCR7 Essentially Contributes to the Homing of Plasmacytoid Dendritic Cells to Lymph Nodes under Steady-State As Well As Inflammatory Conditions. The Journal of Immunology 186, 3364-3372, doi:10.4049/jimmunol.1002598 (2011).

32 Riol-Blanco, L. et al. The Chemokine Receptor CCR7 Activates in Dendritic Cells Two Signaling Modules That Independently Regulate Chemotaxis and Migratory Speed. The Journal of Immunology 174, 4070-4080, doi:10.4049/jimmunol.174.7.4070 (2005).

33 Penna, G., Vulcano, M., Sozzani, S. & Adorini, L. Differential migration behavior and chemokine production by myeloid and plasmacytoid dendritic cells. Human immunology 63, 1164-1171 (2002).

34 Cavanagh, L. L. & Von Andrian, U. H. Travellers in many guises: The origins and destinations of dendritic cells. Immunol Cell Biol 80, 448-462 (2002).

35 Shay, T. & Kang, J. Immunological Genome project and systems immunology. Trends in immunology 34, 602-609, doi:10.1016/j.it.2013.03.004 (2013).

36 Liu, Y.-J. IPC: Professional Type 1 Interferon-Producing Cells and Plasmacytoid Dendritic Cell Precursors. Annual Review of Immunology 23, 275-306, doi:10.1146/annurev.immunol.23.021704.115633 (2005).

37 Lood, C. et al. C1q inhibits immune complex-induced interferon-alpha production in plasmacytoid dendritic cells: a novel link between C1q deficiency and systemic lupus erythematosus pathogenesis. Arthritis and rheumatism 60, 3081-3090, doi:10.1002/art.24852 (2009).

38 ENCODE. The ENCODE (ENCyclopedia Of DNA Elements) Project. Science 306, 636-640, doi:10.1126/science.1105136 (2004).

39 Karrich, J. J. et al. The transcription factor Spi-B regulates human plasmacytoid dendritic cell survival through direct induction of the antiapoptotic gene BCL2- A1. Vol. 119 (2012).

40 Carmona-Sáez, P. et al. Metagene projection characterizes GEN2.2 and CAL-1 as relevant human plasmacytoid dendritic cell models. Bioinformatics (Oxford,

England) 33, 3691-3695, doi:10.1093/bioinformatics/btx502 (2017).

41 Maeda, T. et al. A novel plasmacytoid dendritic cell line, CAL-1, established from a patient with blastic natural killer cell lymphoma. International journal of hematology 81, 148-154 (2005).

42 Ceribelli, M. et al. A Druggable TCF4- and BRD4-Dependent Transcriptional Network Sustains Malignancy in Blastic Plasmacytoid Dendritic Cell Neoplasm. Cancer Cell 30, 764-778, doi:10.1016/j.ccell.2016.10.002 (2016).

43 Bjorck, P. & Kincade, P. W. $CD19^{+}$ pro-B cells can give rise to dendritic cells in vitro. J Immunol 161, 5795-5799 (1998).

44 Izon, D. et al. A common pathway for dendritic cell and early B cell development. J Immunol 167, 1387-1392 (2001).

45 Ghosh, H. S. et al. ETO family protein Mtg16 regulates the balance of dendritic cell subsets by repressing Id2. J Exp Med 211, 1623-1635, doi:10.1084/jem.20132121 (2014).

46 Sasaki, I. et al. Spi-B is critical for plasmacytoid dendritic cell function and development. Blood 120, 4733-4743, doi:10.1182/blood-2012-06-36527 (2012).

47 Zhu, X., Schweitzer, B. L., Romer, E. J., Sulentic, C. E. & DeKoter, R. P. Transgenic expression of Spi-C impairs B-cell development and function by affecting genes associated with BCR signaling. Eur J Immunol 38, 2587-2599, doi:10.1002/eji.200838323 (2008).

48 Li, S. K., Solomon, L. A., Fulkerson, P. C. & DeKoter, R. P. Identification of a negative regulatory role for spi-C in the murine B cell lineage. J Immunol 194, 3798-3807, doi:10.4049/jimmunol.1402432 (2015).

49 Braig, F. et al. Resistance to anti-CD19/CD3 BiTE in acute lymphoblastic leukemia may be mediated by disrupted CD19 membrane trafficking. Blood 129, 100- 104, doi:10.1182/blood-2016-05-718395 (2017).

50 Heidkamp, G. F. et al. Human lymphoid organ dendritic cell identity is predominantly dictated by ontogeny, not tissue microenvironment. Science Immunology 1, doi:10.1126/sciimmunol.aai7677 (2016).

51 Li, S., Wu, J., Zhu, S., Liu, Y. J. & Chen, J. Disease-Associated Plasmacytoid Dendritic Cells. Front Immunol 8, 1268, doi:10.3389/fimmu.2017.01268 (2017).

52 Affandi, A. J., Carvalheiro, T., Radstake, T. & Marut, W. Dendritic cells in systemic sclerosis: Advances from human and mice studies. Immunol Lett, doi:10.1016/j.imlet.2017.11.003 (2017).

53 Kim, D. et al. TopHat2: accurate alignment of transcriptomes in the presence of insertions, deletions and gene fusions. Genome Biol 14, R36, doi:10.1186/gb- 2013-14- 4-r36 (2013).

54 Trapnell, C. et al. Differential analysis of gene regulation at transcript resolution with RNA-seq. Nature biotechnology 31, 46-53, doi:10.1038/nbt.2450 (2013).

55 Iparraguirre, A. et al. Two distinct activation states of plasmacytoid dendritic cells induced by influenza virus and CpG 1826 oligonucleotide. Journal of leukocyte biology 83, 610-620, doi:10.1189/jlb.0807511 (2008).

56 Mootha, V. K. et al. PGC-1alpha-responsive genes involved in oxidative phosphorylation are coordinately downregulated in human diabetes. Nat Genet 34, 267- 273, doi:10.1038/ng1180 (2003).

57 Leylek, R .et al. Integrated cross-species analysis identifies a conserved transitional dendritic cell population. Cell Reports 29, 3736–3750, https://doi.org/10.1016/j.celrep.2019.11.042 (2019).

58 Feng, J. et al. Clonal lineage tracing reveals shared origin of conventional and plasmacytoid dendritic cells. Immunity 3, 405-422.e11, doi: 10.1016/j.immuni.2022.01.016. (2022)

59 Qiu, X. et. al. Reversed graph embedding resolves complex single-cell trajectories. Nat. Methods 14, 979–982, https://doi.org/10.1038/nmeth.4402 (2017)

60 Cao J, Spielmann M, Qiu X, Huang X, Ibrahim DM, Hill AJ, Zhang F, Mundlos S, Christiansen L, Steemers FJ, Trapnell C, Shendure J. The single-cell transcriptional landscape of mammalian organogenesis. Nature. 2019 Feb;566(7745):496-502. doi: 10.1038/s41586-019-0969-x.

61 Nikolic T, Dingjan GM, Leenen PJ, Hendriks RW. A subfraction of B220^{+} cells

in murine bone marrow and spleen does not belong to the B cell lineage but has dendritic cell characteristics. Eur J Immunol. 2002 Mar;32(3):686-92. doi: 10.1002/1521- 4141(200203)32:3<686::AID-IMMU686>3.0.CO;2-I. PMID:11857343.

62 Shapiro-Shelef, M., Calame, K. Regulation of plasma-cell development. Nat Rev Immunol 5, 230–242 (2005). https://doi.org/10.1038/nri1572

63 Edward T Schmid Iris K Pang Eugenio A Carrera Silva Lidia Bosurgi Jonathan J Miner Michael S Diamond Akiko Iwasaki Carla V Rothlin (2016). AXL receptor tyrosine kinase is required for T cell priming and antiviral immunity. eLife 5:e12414. https://doi.org/10.7554/eLife.12414

64 Zhang, D. et al. Axl Mediates Resistance to Respiratory Syncytial Virus Infection Independent of Cell Attachment. Am J Respir Cell Mol Biol 67, 227–240 (2022). https://doi.org/10.1165/rcmb.2021-0362OC

65 Hao Y, Hao S, Andersen-Nissen E, III WMM, Zheng S, Butler A, Lee MJ, Wilk AJ, Darby C, Zagar M, Hoffman P, Stoeckius M, Papalexi E, Mimitou EP, Jain J, Srivastava A, Stuart T, Fleming LB, Yeung B, Rogers AJ, McElrath JM, Blish CA, Gottardo R, Smibert P, Satija R (2021). "Integrated analysis of multimodal single-cell data." Cell. doi:10.1016/j.cell.2021.04.048, https://doi.org/10.1016/j.cell.2021.04.048.

66. Ekiz, H.A., Conley, C.J., Stephens, W.Z., and O'Connell, R.M. (2020). CIPR: a web- based R/shiny app and R package to annotate cell clusters in single cell RNA sequencing experiments. BMC Bioinformatics 21, 191. 10.1186/s12859-020- 3538-2.

67. Dress RJ, Dutertre CA, Giladi A, Schlitzer A, Low I, Shadan NB, Tay A, Lum J, Kairi MFBM,Hwang YY, Becht E, Cheng Y, Chevrier M, Larbi A, Newell EW, Amit I, Chen J, Ginhoux F. Plasmacytoid dendritic cells develop from Ly6D^{+} lymphoid progenitors distinct from the myeloid lineage. Nat Immunol. 2019 Jul;20(7):852-864. doi: 10.1038/s41590-019-0420-3.

68. Nagaharu K, Kojima Y, Hirose H, Minoura K, Hinohara K, Minami H, Kageyama Y, Sugimoto Y, Masuya M, Nii S, Seki M, Suzuki Y, Tawara I, Shimamura T, Katayama N, Nishikawa H, Ohishi K. A bifurcation concept for B-

lymphoid/plasmacytoid dendritic cells with largely fluctuating transcriptome dynamics.Cell Rep. 2022 Aug 30;40(9):111260. doi: 10.1016/j.celrep.2022.111260.

69. Herman JS, Sagar, Grün D. FateID infers cell fate bias in multipotent progenitors from single-cell RNA-seq data. Nat Methods. 2018 May;15(5):379-386. doi: 10.1038/nmeth.4662
70. Rodrigues, P.F., Alberti-Servera, L., Eremin, A. et al. Distinct progenitor lineages contribute to the heterogeneity of plasmacytoid dendritic cells. Nat Immunol 19,711–722 (2018). https://doi.org/10.1038/s41590-018-0136-9
71. Sanjurjo L, Amézaga N, Aran G, Naranjo-Gómez M, Arias L, Armengol C, Borràs FE, Sarrias MR. The human CD5L/AIM-CD36 axis: A novel autophagy inducer in macrophages that modulates inflammatory responses. Autophagy. 2015;11(3):487-502. doi: 10.1080/15548627.2015.1017183. PMID: 25713983; PMCID: PMC4502645.
72. Martinez VG, Escoda-Ferran C, Tadeu Simões I, Arai S, Orta Mascaró M, Carreras E, Martínez-Florensa M, Yelamos J, Miyazaki T, Lozano F. The macrophage soluble receptor AIM/Api6/CD5L displays a broad pathogen recognition spectrum and is involved in early response to microbial aggression. Cell Mol Immunol. 2014 Jul;11(4):343-54. doi: 10.1038/cmi.2014.12. Epub 2014 Mar 3. PMID: 24583716; PMCID: PMC4085514.
73. Nienke Oskam, Maurits den Boer, Marie V. Lukassen, Pleuni Ooijevaar-de Heer, Tim S. Veth, Gerard van Mierlo, Szu-Hsueh Lai, Ninotska I.L. Derksen, Victor C. Yin, Marij Streutker, Vojtech Franc, Marta Siborova, Mirjam Damen, Dorien Kos, Arjan Barendregt, Albert Bondt, Johannes B. van Goudoever, Carla J.C. Haas, Piet C. Aerts, Remy M. Muts, Suzan H.M. Rooijakkers, Gestur Vidarsson, Theo Rispens, Albert J.R. Heck. CD5L is a canonical component of circulatory IgM. bioRxiv 2023.05.27.542462;doi:https://doi.org/10.1101/2023.05.27.542462
74. Wolf, F.A., Hamey, F.K., Plass, M. et al. PAGA: graph abstraction reconciles clustering with trajectory inference through a topology preserving map of single cells. Genome Biol 20, 59 (2019). https://doi.org/10.1186/s13059-019-

1663-x

75. Trapnell C. et. al. The dynamics and regulators of cell fate decisions are revealed by pseudotemporal ordering of single cells. Nat. Biotechnol. 32, 381-386 (2014). https://doi.org/10.1038/nbt.2859

76. Benjamin C. Harman, Juli P. Miller, Neda Nikbakht, Rachel Gerstein, David Allman; Mouse plasmacytoid dendritic cells derive exclusively from estrogen-resistant myeloid progenitors. Blood 2006; 108 (3): 878–885. doi: https://doi.org/10.1182/blood-2005-11-4545

A

Cell Type/100K	WT	cKO	P-value
B cells	19,100 ± 2879	7,633 ± 1426	<0.0001
pDC	1,086 ± 65	626 ± 63	0.0009

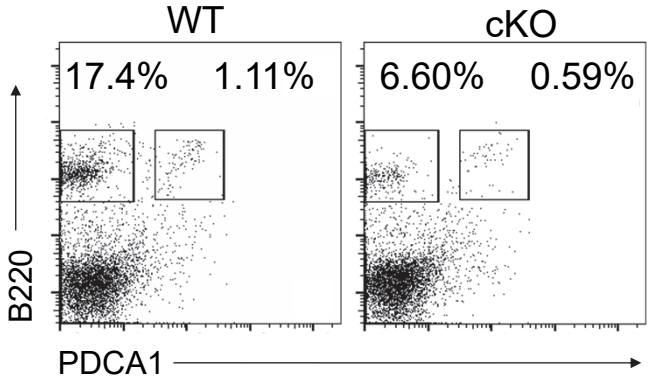

B

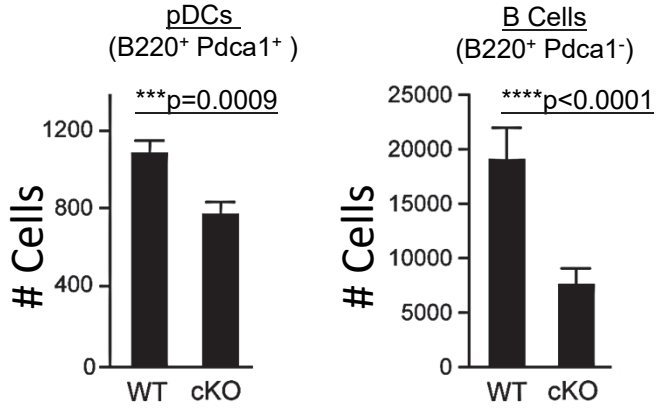

Adoptive Transfer Data

YFP+
YFP−

C

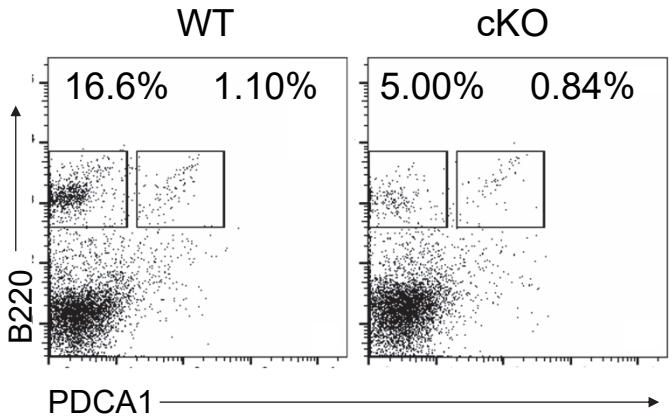

D

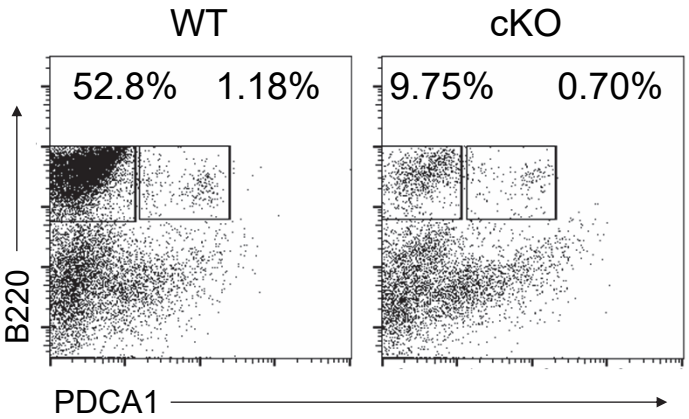

E

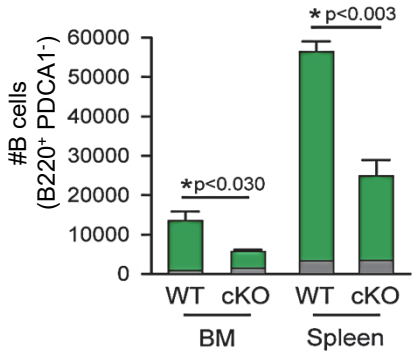

F

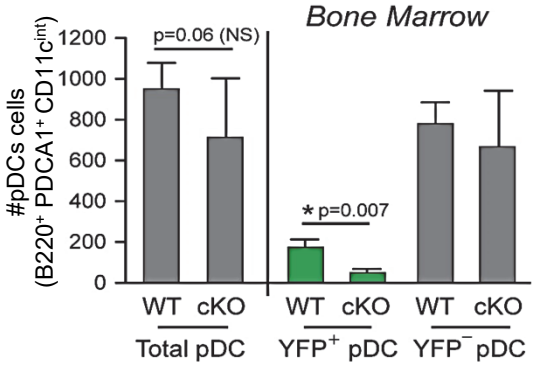

G

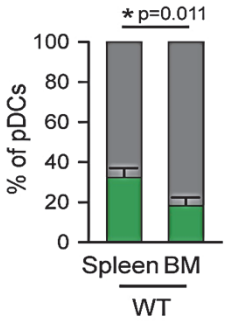

Figure 1

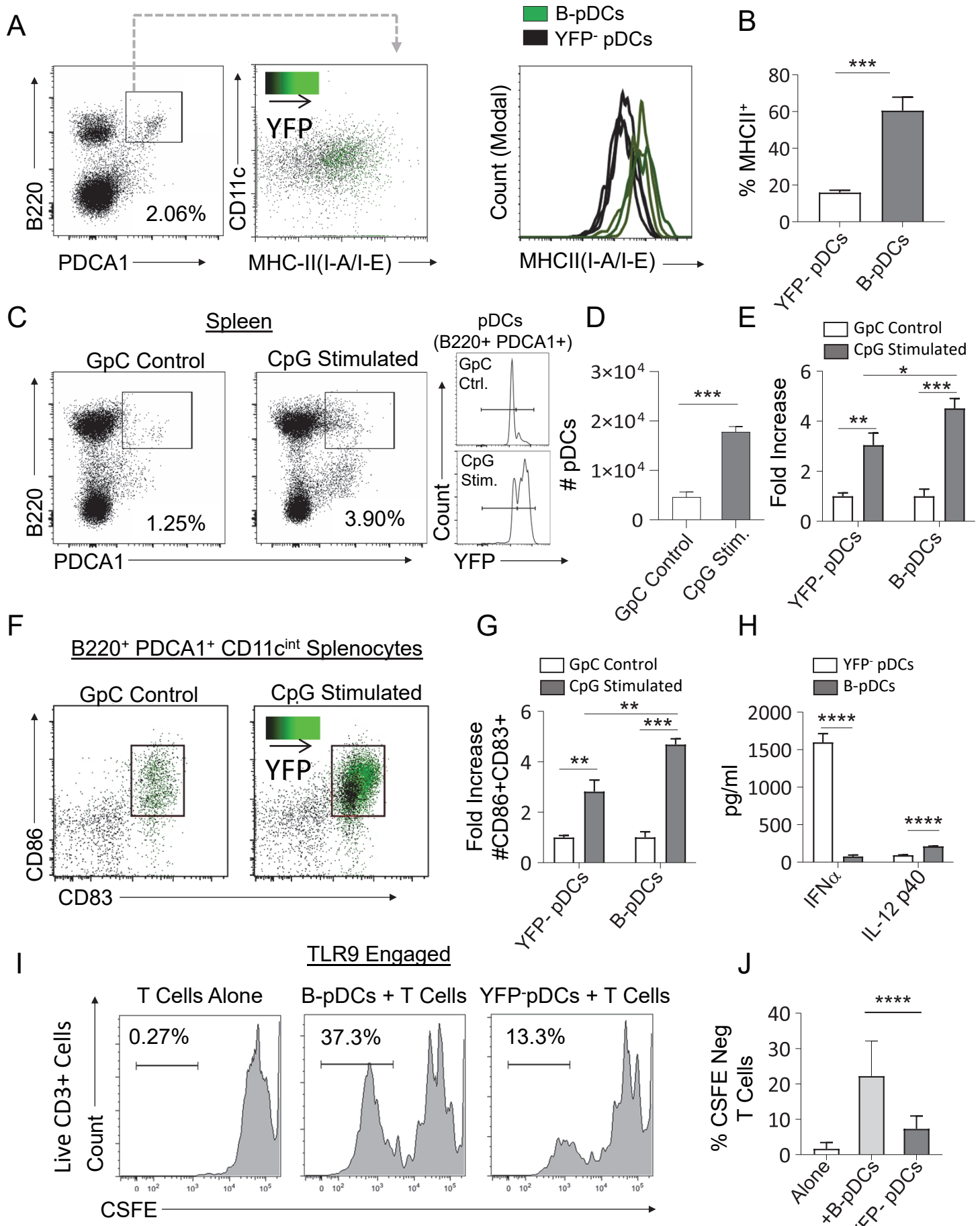
A
B220
PDCA1
2.06%
CD11c
YFP
MHC-II(I-A/I-E)
B-pDCs
YFP- pDCs
Count (Modal)
MHCII(I-A/I-E)
B
% MHCII+
***
YFP- pDCs
B-pDCs
C
Spleen
GpC Control
CpG Stimulated
B220
PDCA1
1.25%
3.90%
pDCs
(B220+ PDCA1+)
GpC
Ctrl.
CpG
Stim.
Count
YFP
D
pDCs
3×10^4
2×10^4
1×10^4
0
***
GpC Control
CpG Stim.
E
GpC Control
CpG Stimulated
Fold Increase
*
***
**
YFP- pDCs
B-pDCs
F
B220+ PDCA1+ CD11c^int Splenocytes
GpC Control
CpG Stimulated
CD86
CD83
YFP
G
GpC Control
CpG Stimulated
Fold Increase
#CD86+CD83+
**
***
YFP- pDCs
B-pDCs
H
YFP- pDCs
B-pDCs
pg/ml
****
IFNα
IL-12 p40
I
TLR9 Engaged
T Cells Alone
B-pDCs + T Cells
YFP-pDCs + T Cells
Live CD3+ Cells
Count
0.27%
37.3%
13.3%
CSFE
J
% CSFE Neg
T Cells
****
Alone
+B-pDCs
+YFP- pDCs

Figure 2

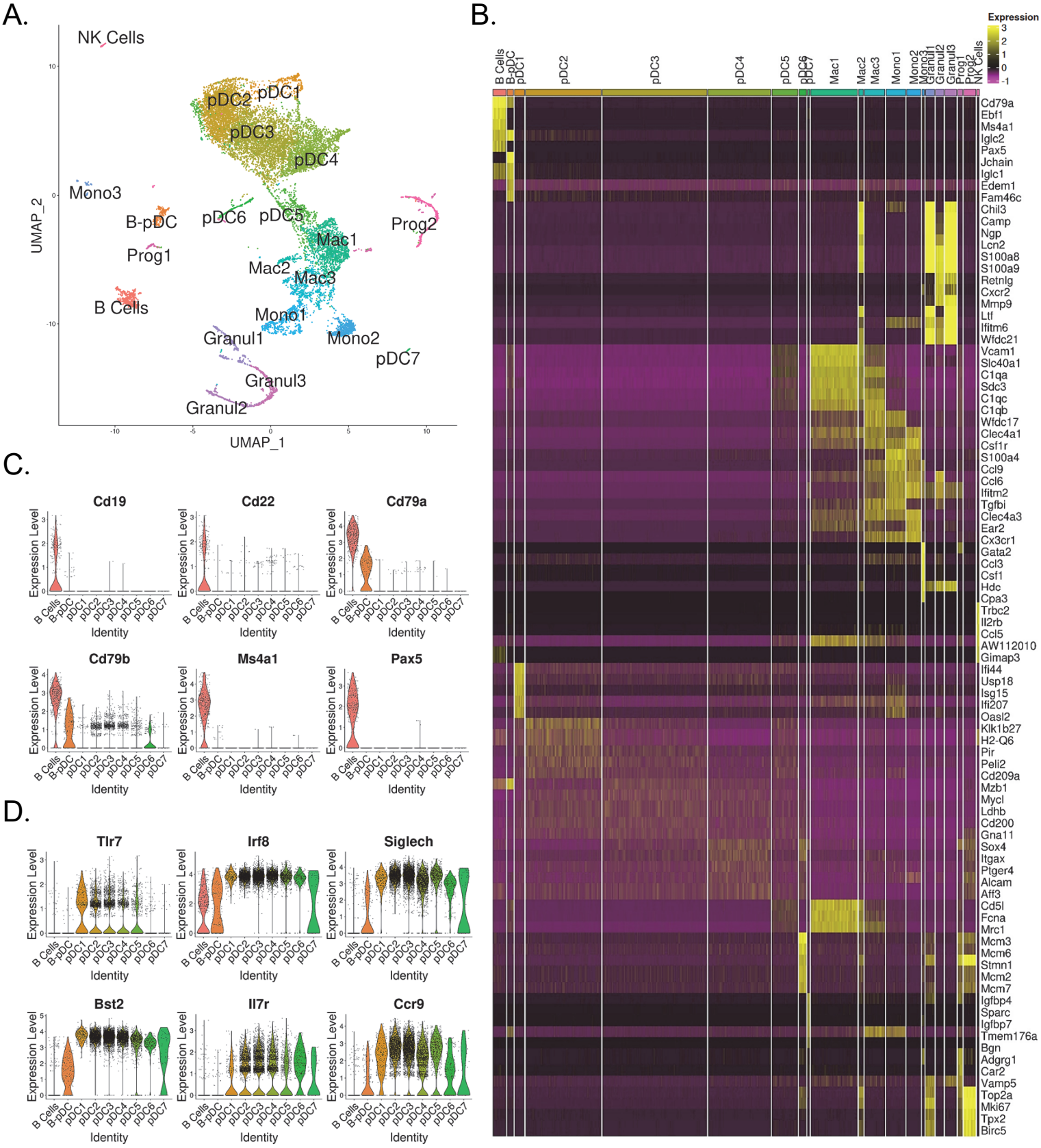
A.
NK Cells
pDC2
pDC1
pDC3
pDC4
Mono3
B-pDC
pDC6
pDC5
Prog2
Mac1
Prog1
Mac2
Mac3
B Cells
Mono1
Granul1
Mono2
pDC7
Granul3
Granul2
UMAP_2
UMAP_1
B.
Expression
B Cells
B-pDC
pDC1
pDC2
pDC3
pDC4
pDC5
pDC6
pDC7
Mac1
Mac2
Mac3
Mono1
Mono2
Mono3
Granul1
Granul2
Granul3
Prog1
Prog2
NK Cells
Cd79a
Ebf1
Ms4a1
Iglc2
Pax5
Jchain
Iglc1
Edem1
Fam46c
Chil3
Camp
Ngp
Lcn2
S100a8
S100a9
Retnlg
Cxcr2
Mmp9
Ltf
Ifitm6
Wfdc21
Vcam1
Slc40a1
C1qa
Sdc3
C1qc
C1qb
Wfdc17
Clec4a1
Csf1r
S100a4
Ccl9
Ccl6
Ifitm2
Tgfbi
Clec4a3
Ear2
Cx3cr1
Gata2
Ccl3
Csf1
Hdc
Cpa3
Trbc2
Il2rb
Ccl5
AW112010
Gimap3
Ifi44
Usp18
Isg15
Ifi207
Oasl2
Klk1b27
H2-Q6
Pir
Peli2
Cd209a
Mzb1
Mycl
Ldhb
Cd200
Gna11
Sox4
Itgax
Ptger4
Alcam
Aff3
Cd5l
Fcna
Mrc1
Mcm3
Mcm6
Stmn1
Mcm2
Mcm7
Igfbp4
Sparc
Igfbp7
Tmem176a
Bgn
Adgrg1
Car2
Vamp5
Top2a
Mki67
Tpx2
Birc5
C.
Cd19
Cd22
Cd79a
Cd79b
Ms4a1
Pax5
Expression Level
Identity
D.
Tlr7
Irf8
Siglech
Bst2
Il7r
Ccr9
Expression Level
Identity

Figure 3

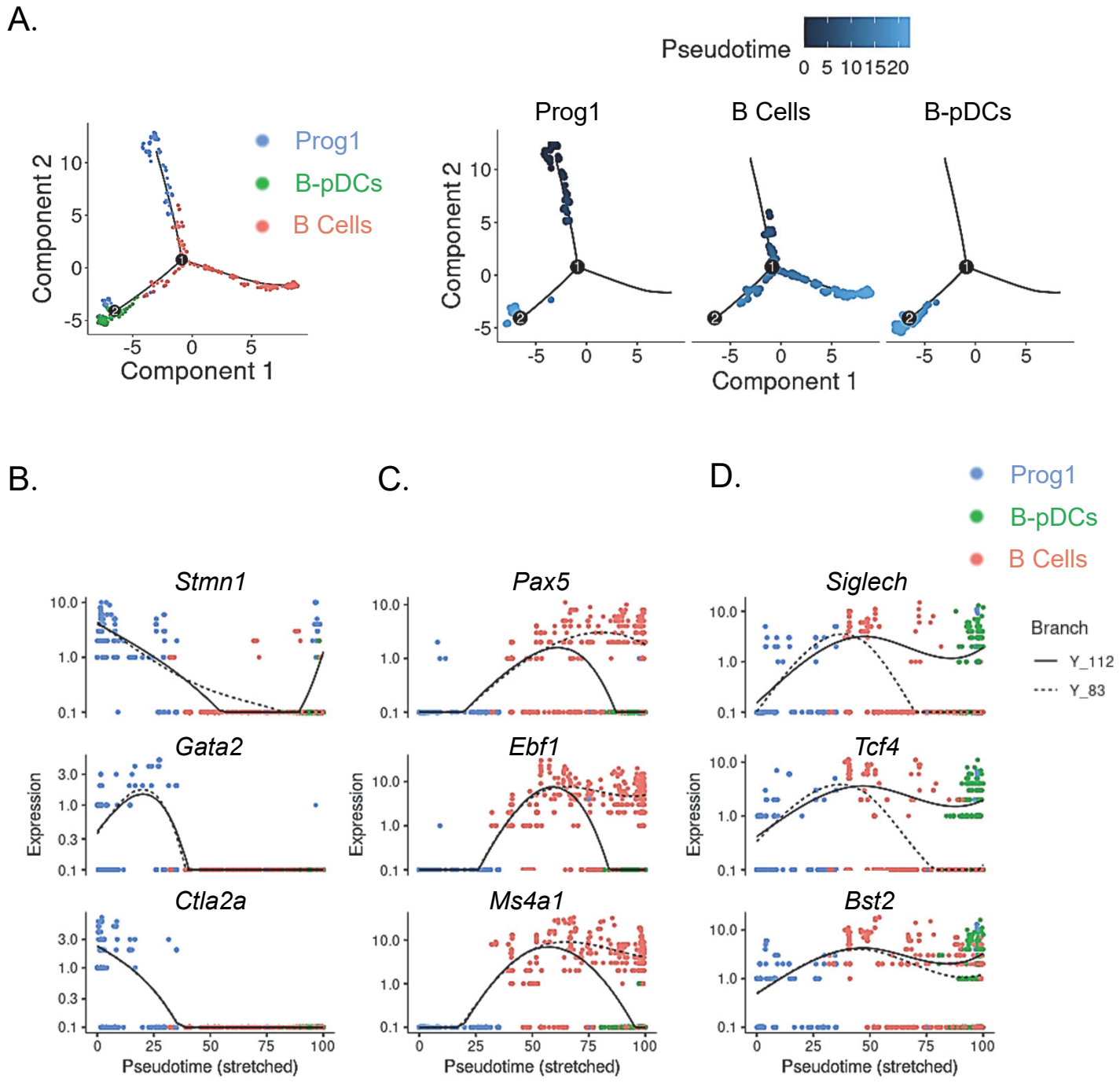
A.
Pseudotime
0 5 10 15 20
Prog1
B-pDCs
B Cells
Component 2
Component 1
Prog1
B Cells
B-pDCs
B.
C.
D.
Prog1
B-pDCs
B Cells
Stmn1
Pax5
Siglech
Gata2
Ebf1
Tcf4
Ctla2a
Ms4a1
Bst2
Expression
Pseudotime (stretched)
Branch
Y_112
Y_83

Figure 4

A.

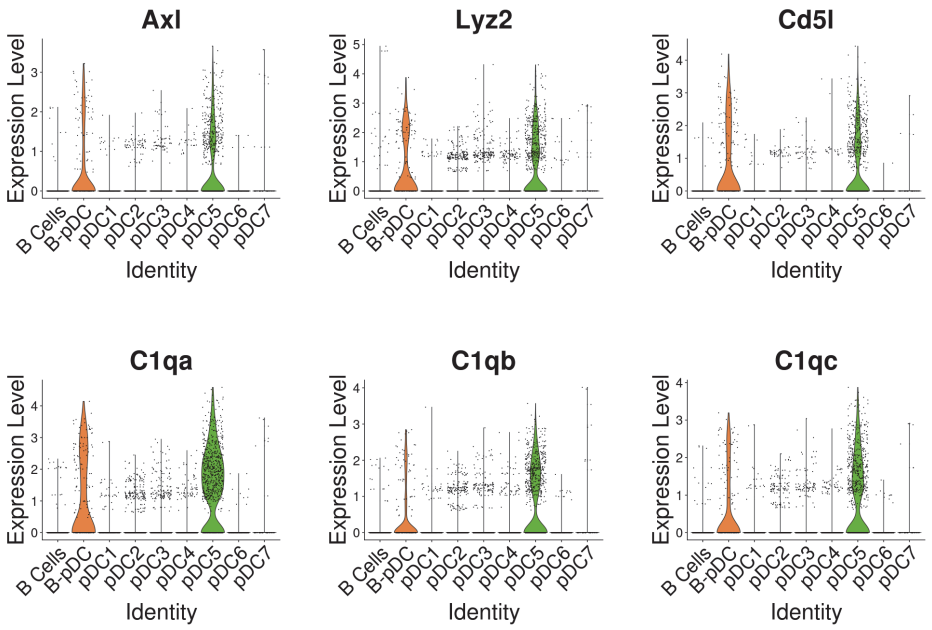
Axl
Lyz2
Cd5l
C1qa
C1qb
C1qc
Expression Level
Identity
B Cells
B-pDC
pDC1
pDC2
pDC3
pDC4
pDC5
pDC6
pDC7

B.

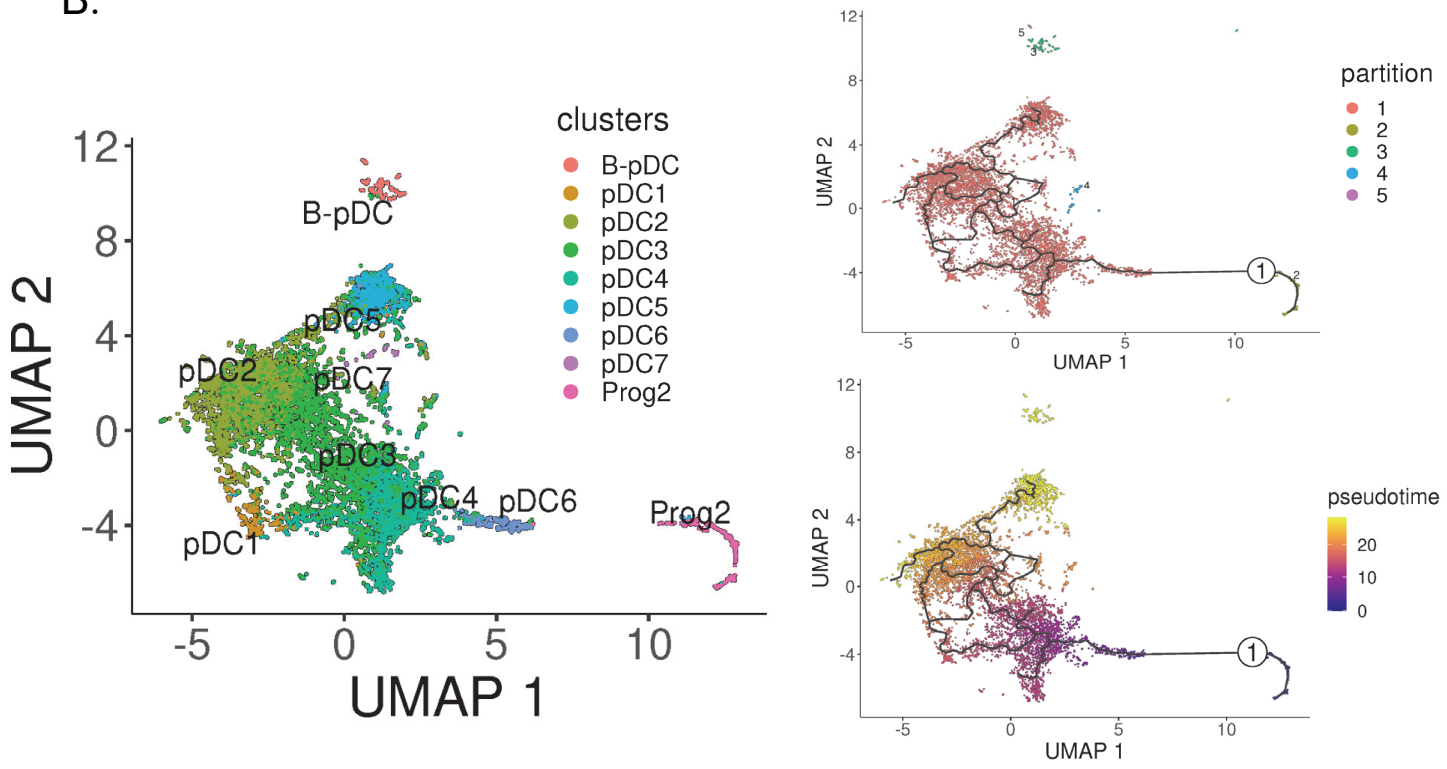
clusters
B-pDC
pDC1
pDC2
pDC3
pDC4
pDC5
pDC6
pDC7
Prog2
UMAP 1
UMAP 2
partition
1
2
3
4
5
pseudotime
20
10
0

Figure 5

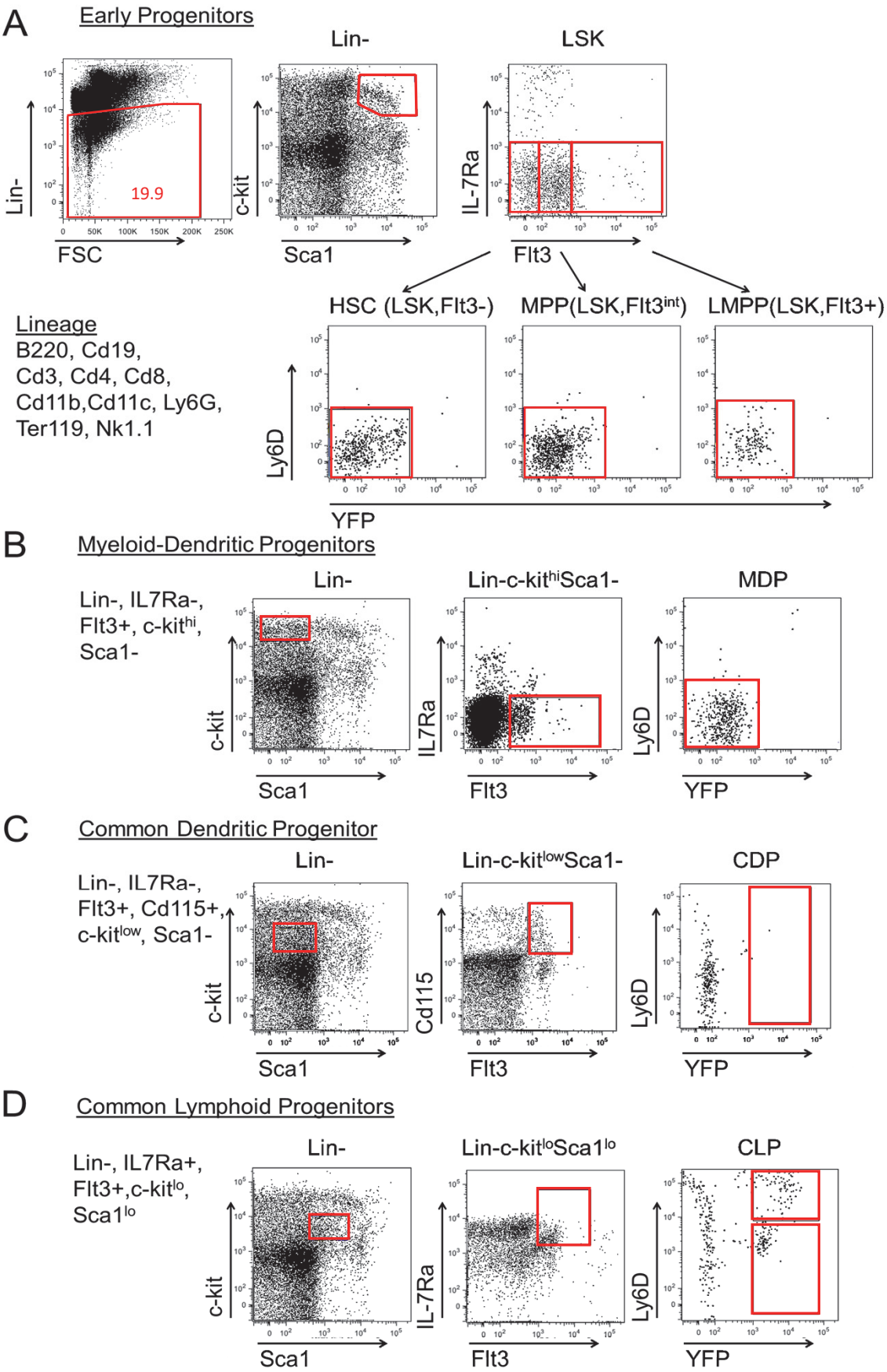

Supplemental Figure 1

A

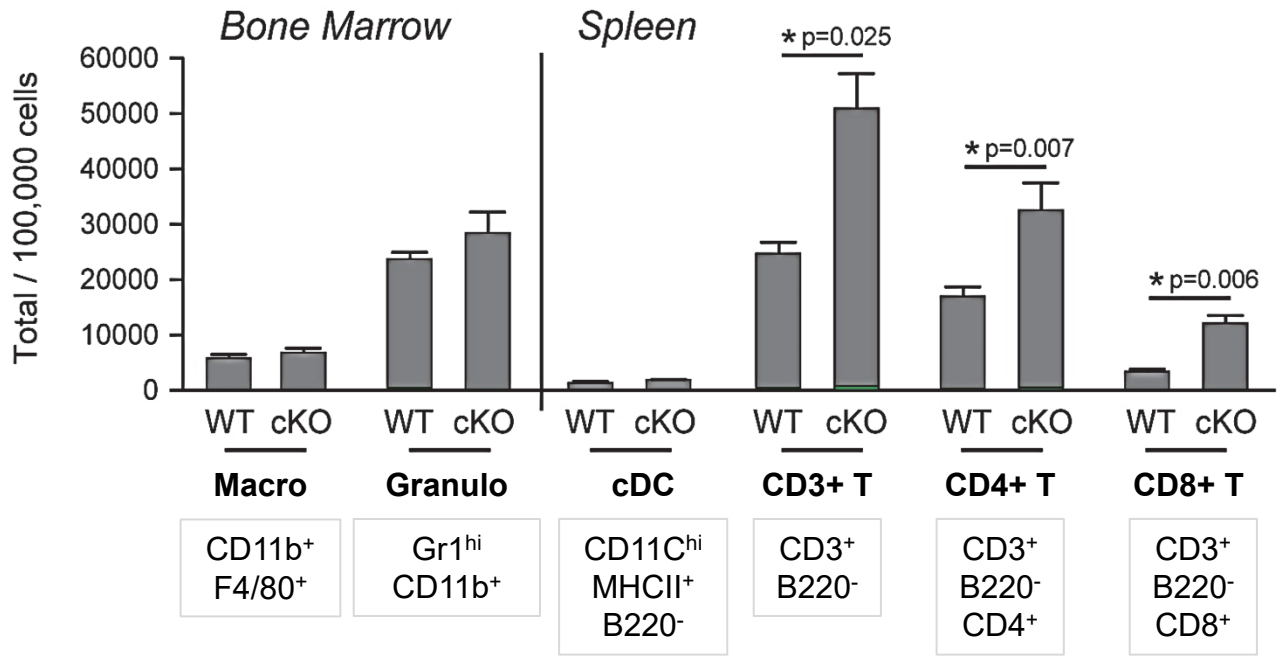

Supplemental Figure 2

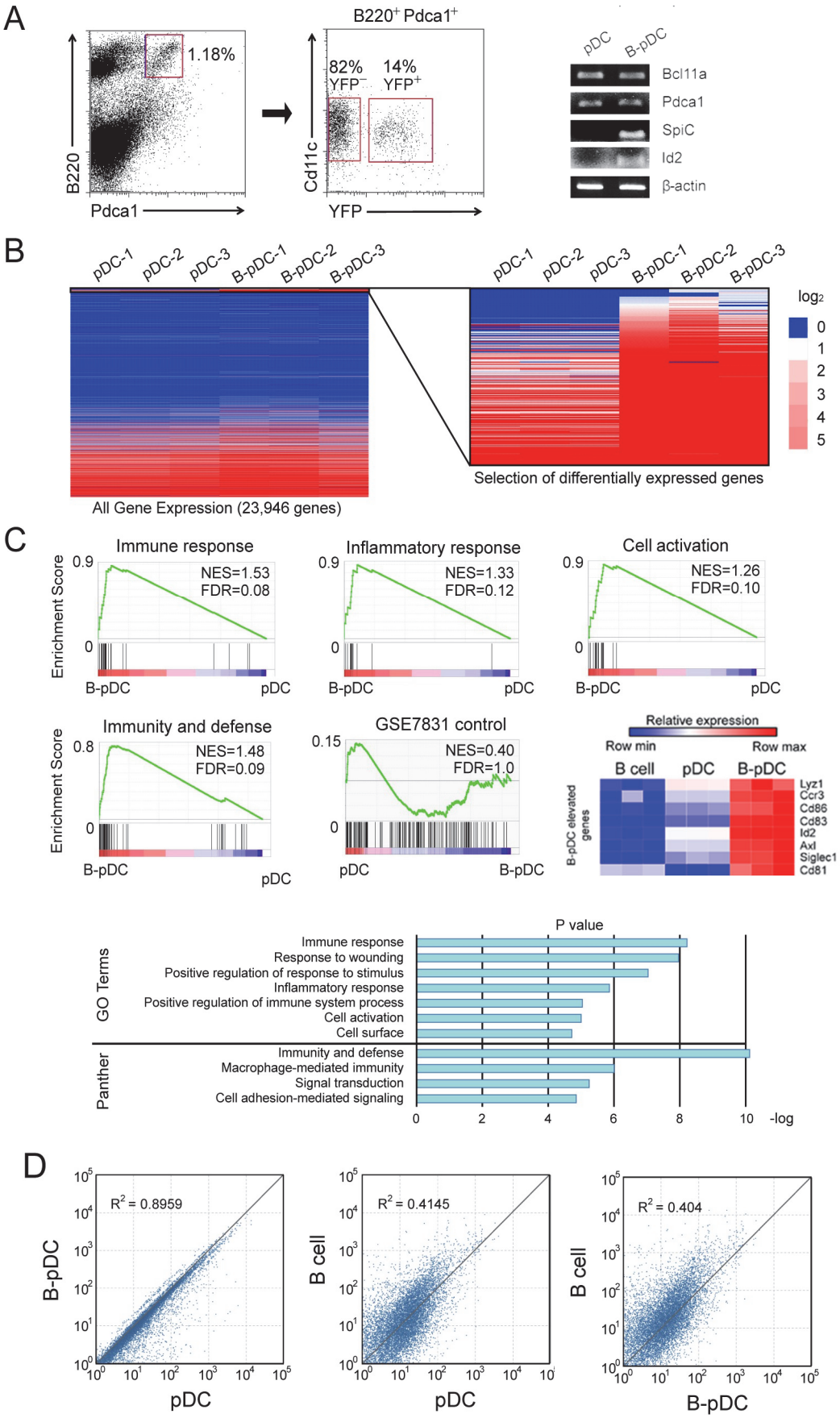

Supplemental Figure 3

A

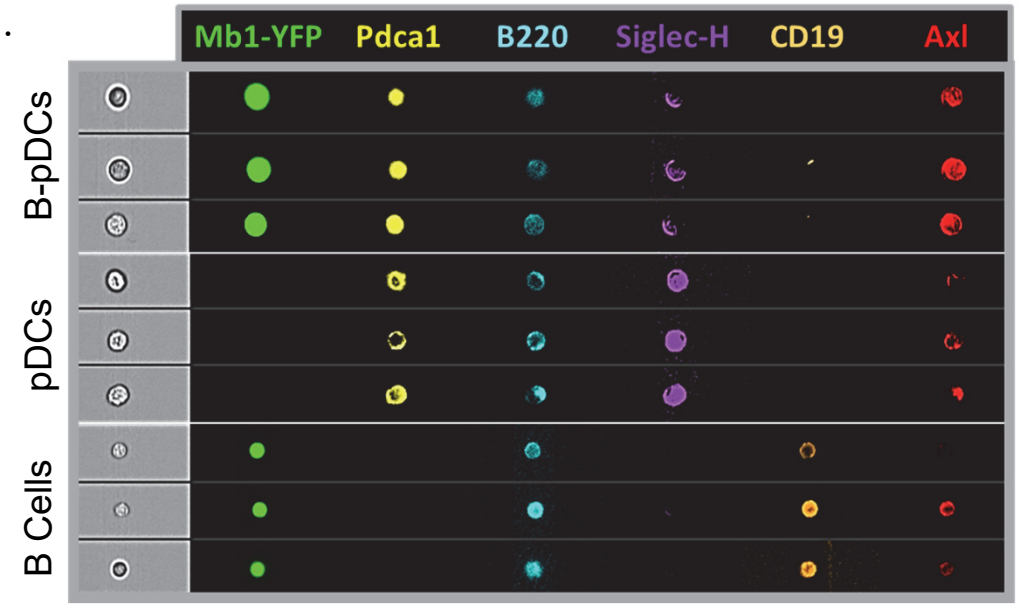

B.

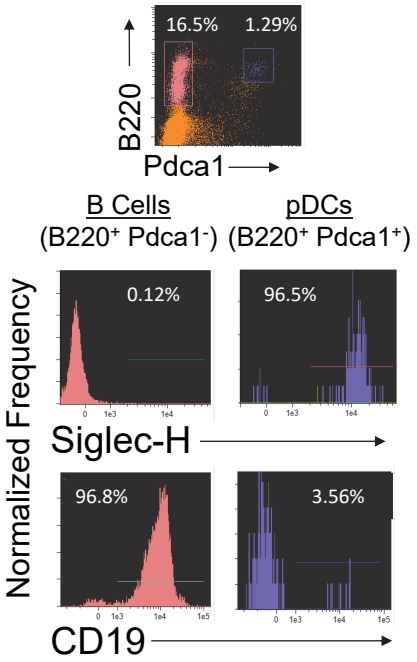

C.

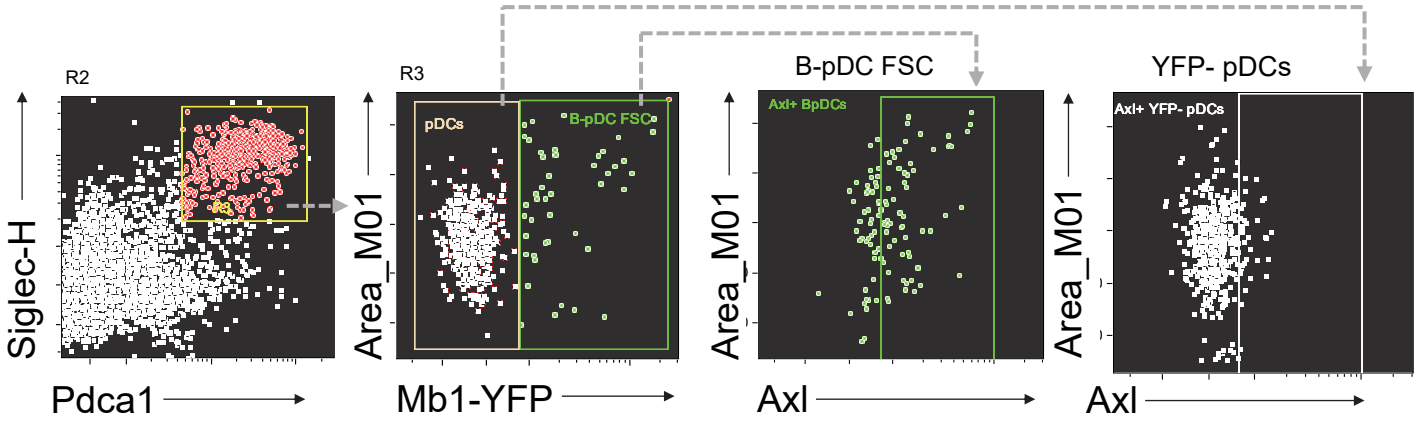

D.

	In Focus		All pDCs		BpDCs		Axl+ BpDCs		YFP- pDCs		Axl+ YFP- pDCs	
Gating Hierarchy	R2 & R1		R2 & R1 : PDCA1+SiglecH+		R2 & R1 : PDCA1+SiglecH+ : Area_M01: Mb1-YFP+		R2 & R1 : PDCA1+SiglecH+ : Area_M01: Mb1-YFP+: Area_M01: Axl+		R2 & R1 : PDCA1+SiglecH+ : Area_M01: Mb1-YFP-		R2 & R1 : PDCA1+SiglecH+ : Area_M01: Mb1-YFP-: Area_M01: Axl+	
Sample	Count	% Gated	Count	% Gated	Count	% Gated	Count	% Gated	Count	% Gated	Count	% Gated
01_WT BM unstained_1	7838	100	0	0	0	0	0	0	0	0	0	0
02_WT BM stained_2	7627	99.9	127	1.67	1	0.79	124	97.6	124	97.6	18	14.5
03_YFP BM unstained_3	7781	100	3	0.04	1	33.3	0	0	2	66.7	0	0
04_YFP BM stained_4	7603	99.9	137	1.8	15	10.9	6	40	113	82.5	31	27.4
05_YFP BM_5	40063	99.9	694	1.73	149	21.5	87	58.4	534	76.9	37	6.93
06_YFP BM_6	39032	99.6	654	1.68	111	17	58	52.3	527	80.6	36	6.83
07_YFP BM_7	13988	98.9	145	1.04	34	23.4	16	47.1	110	75.9	11	10
08_YFP BM_8	31694	98.8	509	1.61	73	14.3	43	58.9	364	71.5	49	13.5
09_YFP BM_9	16022	99.9	208	1.3	25	12	16	64	179	86.1	17	9.5

E.

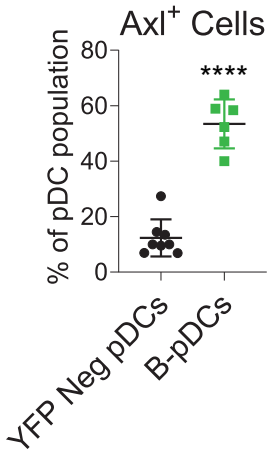

Supplemental Figure 4

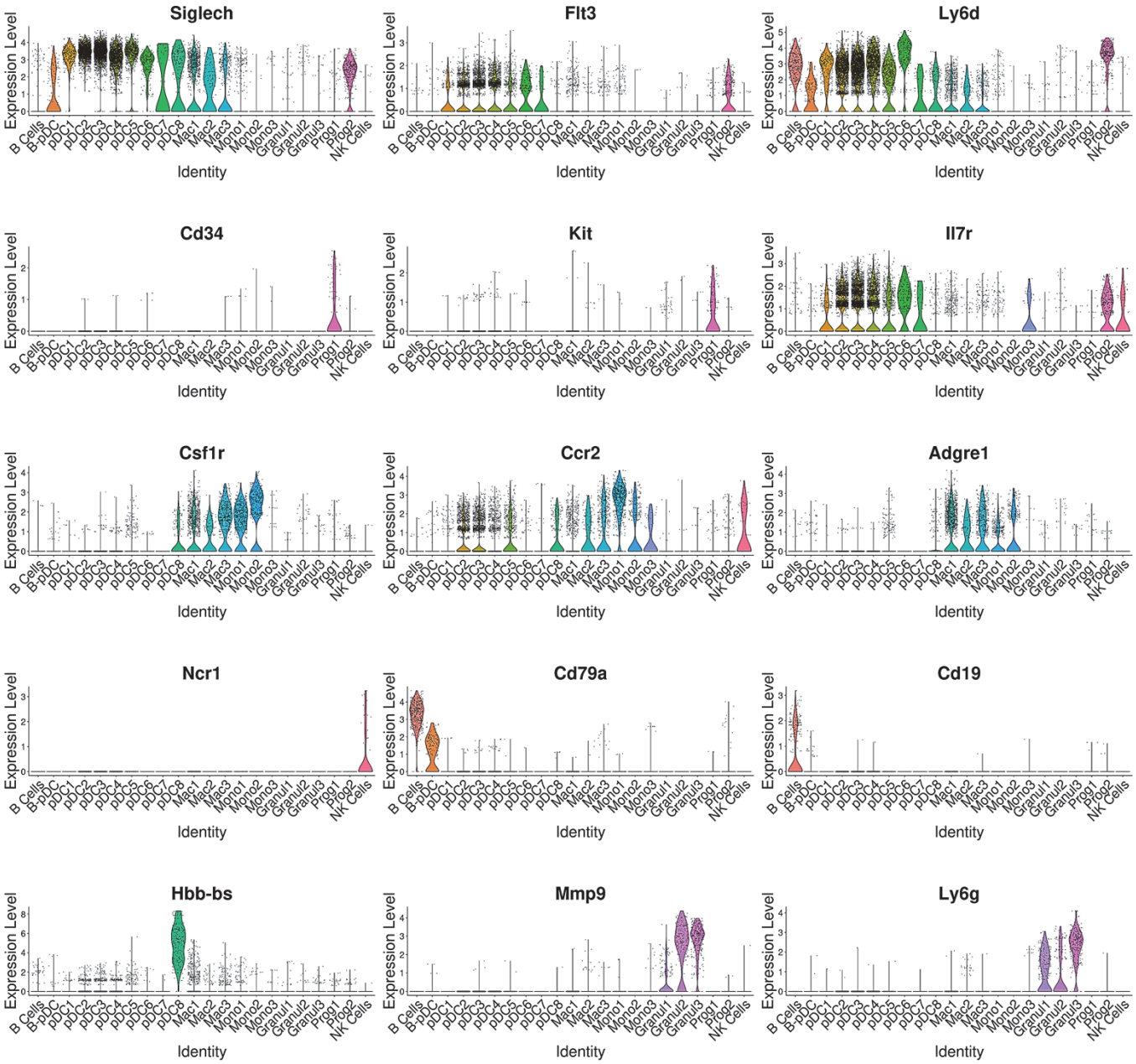

Supplemental Figure 5

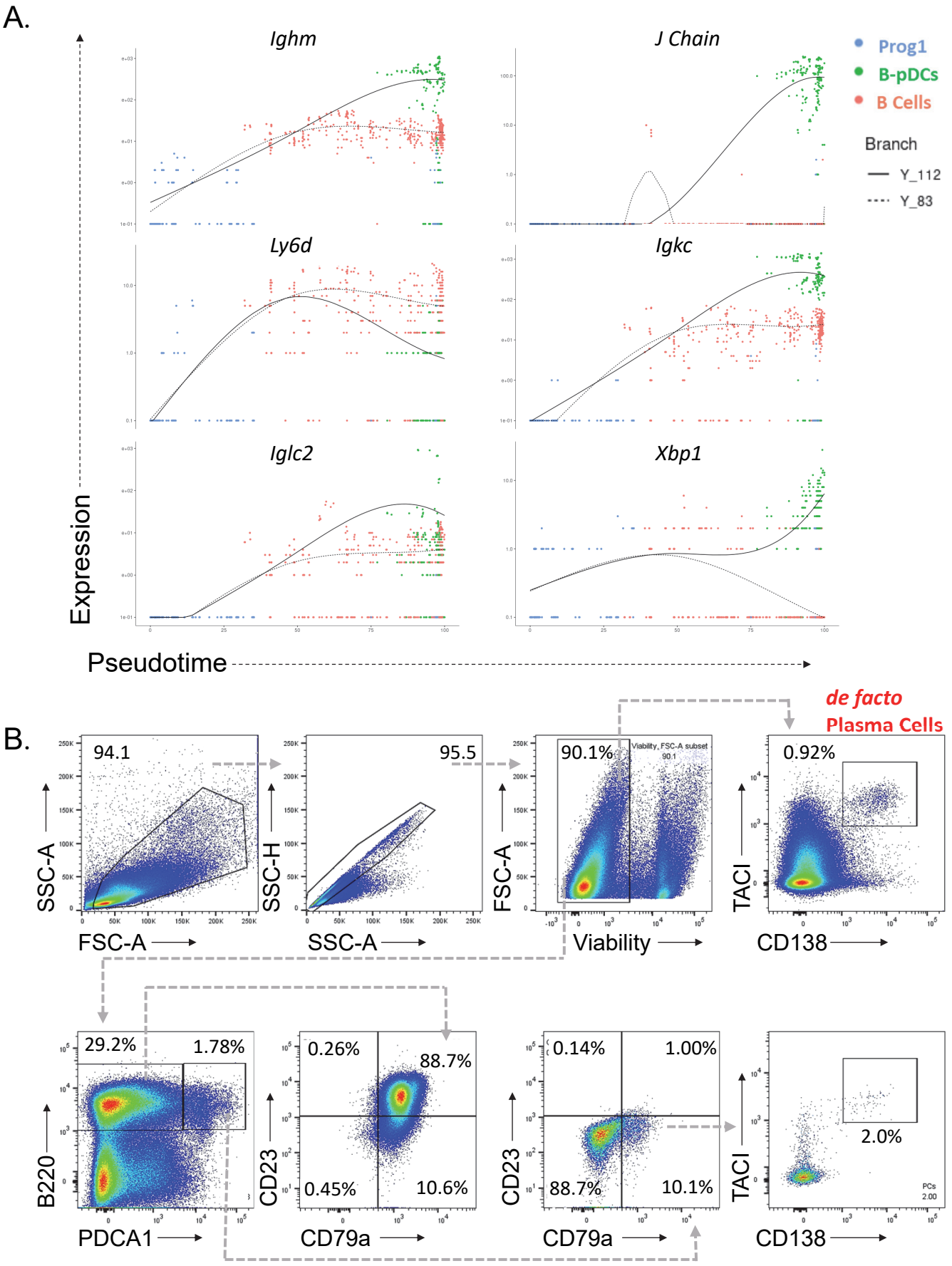

Supplemental Figure 6

A

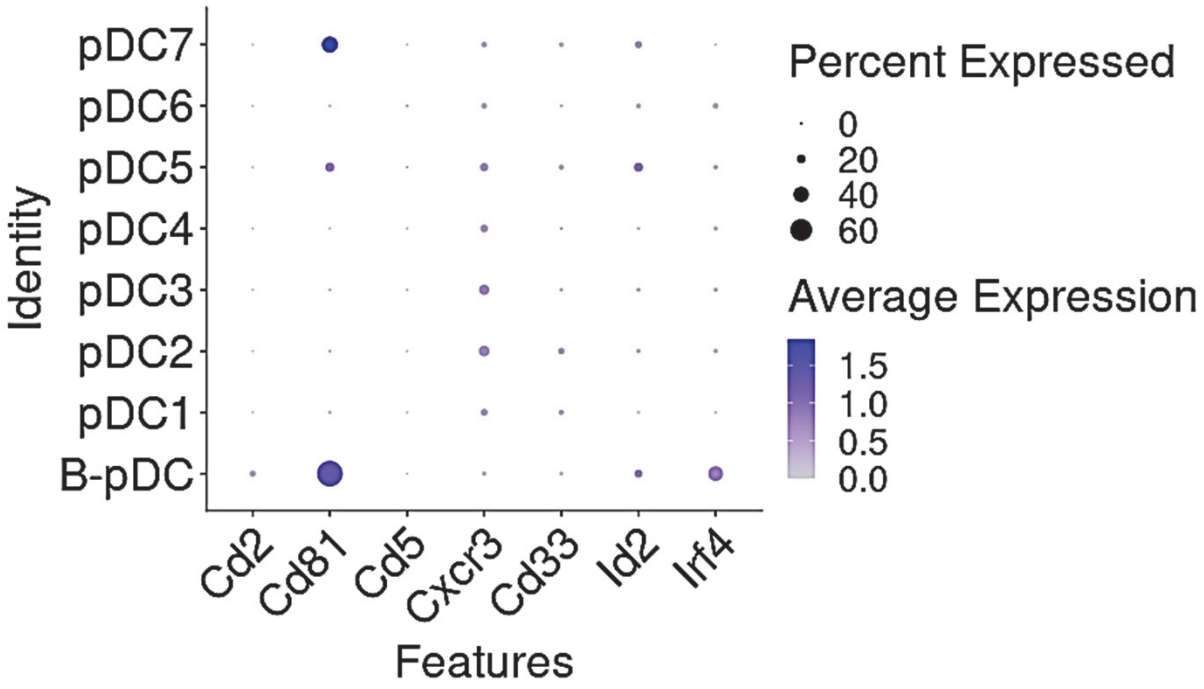

B

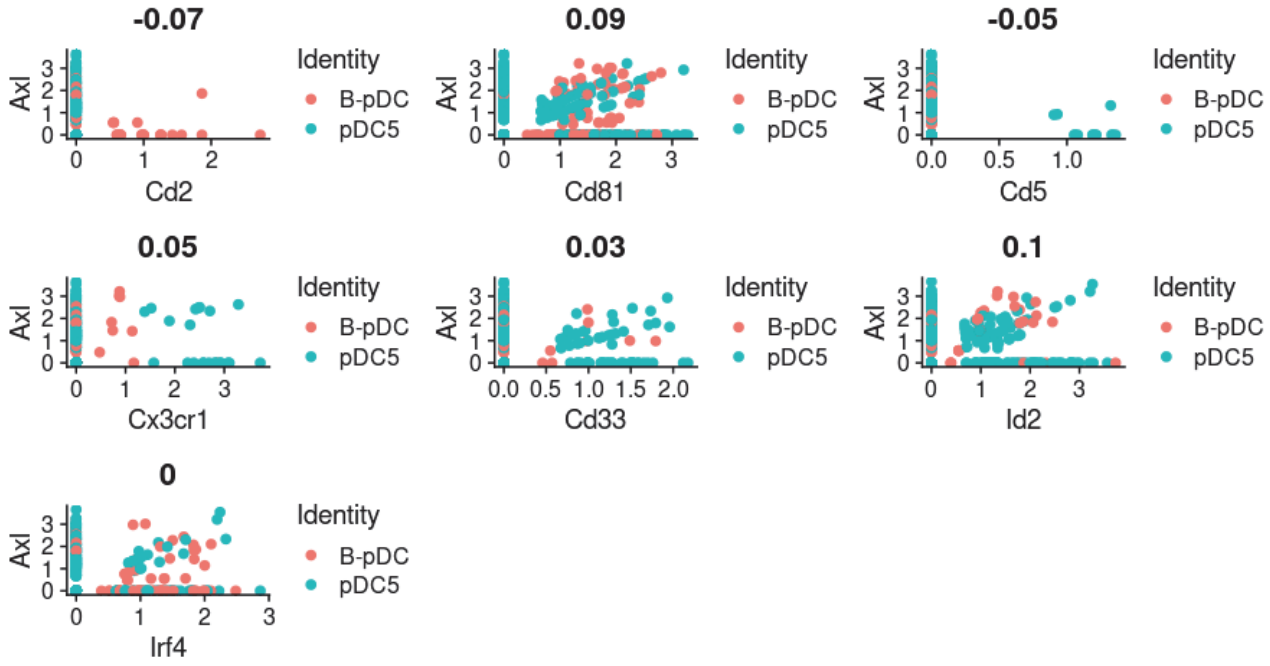

Supplemental Figure 7

Cluster	Ref. Cell Type	CIPR Ref. ID	Consensus ID	ID Score	Z Score
X0	DC	DC.pDC.8-.Sp	pDC3	0.87	2.92
X1	DC	DC.pDC.8-.Sp	pDC2	0.87	3.05
X2	DC	DC.pDC.8-.Sp	pDC4	0.86	2.69
X3	Macrophage	MF.Thio5.II+480	Mac1	0.79	2.46
X4	DC	DC.pDC.8-.Sp	pDC5	0.84	2.88
X5	Macrophage	MF.11cloSer.SI	Mac3	0.82	2.40
X6	Monocyte	Mo.6+2+.BL	Mono1	0.84	2.55
X7	Monocyte	Mo.6C-IIint.Bl	Mono2	0.85	3.02
X8	B cell	B.Fo.Sp	B Cells	0.82	1.93
X9	Stem-Progenitor	SC.CDP.BM	Prog2	0.83	2.16
X10	Granulocyte	GN.BM	Granul3	0.81	3.41
X11	DC	DC.pDC.8-.Sp	pDC1	0.84	3.10
X12	Granulocyte	GN.BM	Granul1	0.76	2.18
X13	DC	DC.pDC.8-.Sp	pDC8	0.75	2.19
X14	Granulocyte	GN.BM	Granul2	0.75	2.74
X15	DC	DC.pDC.8-.Sp	pDC6	0.81	1.91
X16	DC	DC.pDC.8-.Sp	B-pDC	0.75	2.25
X17	Macrophage	MF.II+480lo.PC	Mac2	0.75	2.11
X18	Stem-Progenitor	MLP.BM	Prog1	0.79	2.18
X19	NK cell	NK.DAP10-.Sp	NK Cells	0.72	1.41
X20	Monocyte	Mo.6C+II-.LN	Mono3	0.69	1.73
X21	DC	DC.pDC.8-.Sp	pDC7	0.62	2.97

Supplemental Table 1

Marker	p_val	avg_log2FC	pct.1	pct.2	p_val_adj
Jchain	0	8.374583	0.968	0.01	0
Iglc1	0	7.384079	0.753	0.024	0
Iglc2	0	6.93436	0.876	0.039	0
Ckap4	0	2.288614	0.817	0.05	0
Cd79a	0	2.130392	0.683	0.005	0
Iglv1	0	2.07227	0.366	0	0
Derl3	0	1.951565	0.608	0.007	0
Chst1	0	1.843237	0.478	0	0
Cd81	0	1.748841	0.731	0.045	0
Pou2af1	0	1.408274	0.511	0.001	0
Prg2	0	1.221508	0.484	0.002	0
Eaf2	0	1.203375	0.495	0.011	0
Fkbp11	0	0.971198	0.425	0.007	0
Cacna1s	0	0.816281	0.376	0.004	0
Tnfrsf17	0	0.810065	0.306	0.001	0
Lax1	0	0.653721	0.333	0.004	0
Rapgef3	0	0.63881	0.317	0.002	0
Oosp1	0	0.549178	0.306	0	0
Cacna1h	0	0.3548	0.274	0	0
Fam46c	1.94E-290	1.973402	0.758	0.059	3.13E-286
Prdm1	5.50E-274	0.655727	0.29	0.006	8.90E-270
St8sia6	1.28E-266	0.668541	0.269	0.005	2.07E-262
Igha	3.09E-214	8.551656	0.328	0.013	5.00E-210
Slamf7	5.60E-210	1.233262	0.527	0.038	9.07E-206
Egr1	5.09E-205	1.653236	0.505	0.035	8.24E-201
Igkc	1.18E-157	9.329484	0.935	0.258	1.91E-153
Ikzf3	9.76E-139	0.655167	0.339	0.022	1.58E-134
Atxn1	5.14E-137	0.502322	0.274	0.014	8.32E-133
Edem1	6.09E-130	2.247955	0.833	0.192	9.86E-126
Dennd5b	3E-121	1.202647	0.5	0.06	4.8E-117
Serpina3g	8.8E-111	0.446503	0.258	0.016	1.4E-106
Kcnn4	1.3E-110	0.746446	0.473	0.056	2.1E-106
Ptpn22	1.7E-109	0.487952	0.263	0.017	2.7E-105
Bst2	1.9E-107	-2.55211	0.812	0.981	3E-103
Tmem176b	4.5E-104	1.21053	0.581	0.094	7.2E-100
Tram2	1.8E-100	0.898306	0.435	0.052	2.87E-96
Tyrobp	2.8E-100	-2.93301	0.543	0.966	4.46E-96
Rgcc	8.2E-100	0.698419	0.392	0.043	1.32E-95
Plac8	1.1E-99	-2.74335	0.532	0.968	1.79E-95
Fau	1.1E-99	-1.51384	0.978	0.99	1.8E-95
Tmem176a	2.11E-94	1.147371	0.505	0.078	3.42E-90
Siglech	2.15E-94	-2.43541	0.435	0.975	3.48E-90
Rpl19	5.61E-93	-1.60971	0.898	0.974	9.08E-89
Rpl31	6.64E-93	-2.11381	0.726	0.969	1.07E-88
Rpl30	3.32E-92	-1.46995	0.919	0.984	5.38E-88
Man1a	5.39E-92	0.950944	0.516	0.078	8.73E-88
Mzb1	1.5E-91	2.698237	0.844	0.311	2.42E-87
Rps11	1.83E-90	-1.62328	0.93	0.983	2.95E-86
Rpl18a	2.41E-90	-1.47776	0.898	0.981	3.89E-86

Supplemental Table 2